SCLEROCHRONOLOGICAL EVIDENCE OF LIFE HISTORY AND AMBIENT TEMPERATURE FROM MODERN AND EARLY PLEISTOCENE *GLYCYMERIS AMERICANA* (MOLLUSCA:BIVALVIA) OF THE U.S. EASTERN SEABOARD

ANDREW L.A. JOHNSON,[1] BERND R. SCHÖNE,[2] MELANIE J. LENG,[3] TRIPTI BHATTACHARYA,[4] DAVID K. MOSS,[5] LINDA C. IVANY[4] and RICHARD P. DUFF[1]

[1]*School of Science, University of Derby, Derby DE22 1GB, United Kingdom;*

[2]*Institute of Geosciences, University of Mainz, 55128 Mainz, Germany;*

[3]*National Environmental Isotope Facility, British Geological Survey, Keyworth NG12 5GG, United Kingdom;*

[4]*Department of Earth and Environmental Sciences, Syracuse University, Syracuse, NY 13244, USA;*

[5]*Department of Environmental and Geosciences, Sam Houston State University, Huntsville, TX 77341, USA*

email: a.l.a.johnson@derby.ac.uk

ABSTRACT: Growth-increment and isotopic studies of shells of the marine bivalve *Glycymeris americana* are a potential source of information bearing on its life history and preferred environment over the late Cenozoic on the U.S. eastern seaboard. We demonstrate that the ages of shells can be determined from growth bands and ontogenetic profiles of oxygen isotope ($\delta^{18}O$) composition, and that shell aragonite is deposited in oxygen isotopic equilibrium with seawater, enabling calculation of ambient temperatures by means of a generic transfer function. Modern specimens from North Carolina rarely reach the large size commonly attained by modern forms from Florida and early Pleistocene forms from both states, and modern populations from North Carolina probably include fewer old individuals, the most certain disparity being with early Pleistocene populations from the state. The temporal change in age structure in North Carolina may be an effect of recent scallop trawling but earlier non-anthropogenic environmental change cannot be ruled out as the cause. Maximum and minimum temperatures calculated from the $\delta^{18}O$ profiles of early Pleistocene shells indicate a larger seasonal range than now in both Florida and North Carolina, due to cooler winters. This may reflect greater southward penetration of cool northern waters, with transport along the shelf supplemented by upwelling of water brought south at depth.

INTRODUCTION

Glycymeris da Costa is a genus of non-siphonate, shallow-burrowing arcoid bivalves that evolved from cucullaeid arcoids in the Cretaceous (Cox et al. 1969; Thomas 1975) and, as recorded in the Ocean Biodiversity Information System (OBIS, undated), now occurs worldwide in tropical and temperate marine shelf settings. The genus is a common element in fossil assemblages representing these environments from the Neogene onwards. The aragonite shell (particularly the interior of the hinge plate, which serves as the attachment surface for the ligament and bears the taxodont teeth) generally shows a good record of annual increments. For this reason *Glycymeris* has attracted much attention from sclerochronologists, who have used the increment information to construct multi-

decadal to multi-centennial (multi-individual) chronologies and to determine life and environmental histories (Peharda et al. 2012, 2016; Brocas et al. 2013; Reynolds et al. 2013, 2017a, 2017b; Royer et al. 2013; Bušelić et al. 2015; Moss et al. 2016; Yamaoka et al. 2016; Beaver et al. 2017; Featherstone et al. 2017; Nemeth and Kern 2018; Gimenez et al. 2020; Alexandroff et al. 2021; Johnson et al. 2021). In many of these studies, increment information has been supplemented by oxygen isotope ($\delta^{18}O$) profiles to test the annual periodicity of bounding growth lines and supply temperature estimates. Some further studies of *Glycymeris* have been largely or entirely based on $\delta^{18}O$ data (Berthou et al. 1986; Walliser et al. 2015, 2016; Crippa et al. 2016; Peharda et al. 2019a, 2019b; Featherstone et al. 2020; Johnson et al. 2022).

Most $\delta^{18}O$ thermometry using *Glycymeris* has employed the generic aragonite equation of Grossman and Ku (1986). However, Royer et al. (2013) determined a species-specific equation applicable to modern *Glycymeris glycymeris* from Brittany (France). This equation, implying non-equilibrium isotopic incorporation, was subsequently used by Featherstone et al. (2020) for further work on modern *G. glycymeris* in Brittany and (in a comparison with results derived using the Grossman and Ku equation) by Reynolds et al. (2017a) for work in north-west Scotland; it has also been used for work on Oligocene *G. obovata* and *G. planicostalis* (Walliser et al. 2016). The equations of Grossman and Ku (1986) and Royer et al. (2013) yield significantly different estimates for seasonal temperatures and annual range from the same shell (and water) $\delta^{18}O$ values so it is important to know which equation is the better one to use in *Glycymeris*-based $\delta^{18}O$ thermometry (Reynolds et al. 2017a; Johnson et al. 2022).

A potentially useful *Glycymeris* species for $\delta^{18}O$ thermometry is *G. americana*, an apparently long-lived form (Johnson et al. 2021) that occurs in Neogene to present-day shelf assemblages on the eastern seaboard of the United States and farther south (Porter and Wolfe 1971; Campbell 1993; Abbott and Morris 1995). However, to date there has been no study of modern forms to determine whether or not isotopic incorporation in *G. americana* departs from equilibrium. We remedy this deficiency herein and go on to provide some initial temperature estimates from early Pleistocene

forms. We also use the $\delta^{18}O$ data to test whether the growth increments in the hinge plate of *G. americana* are annual, and proceed to make some preliminary interpretations of life history at present and in the early Pleistocene from counts and measurements of hinge increments and of cycles in $\delta^{18}O$ profiles. Life history information is of potential value for conservation of marine bivalve species (Schöne et al. 2003; Kirby and Miller 2005; Lockwood and Mann 2019; Hesterberg et al. 2020; Killam et al. 2021; Palmer et al. 2021) and is particularly worth obtaining for *G. americana* since it may be approaching extinction (Nicol 1953).

G. AMERICANA (DEFRANCE, 1826): BACKGROUND INFORMATION

G. americana (Fig. 1) belongs to the group of *Glycymeris* species (including *G. glycymeris*) with numerous low, striated ribs (Thomas 1975). It appears at approximately the same time in the late Pliocene throughout the US Atlantic and Gulf Coastal Plain from Virginia and North Carolina (Rushmere Member of the Yorktown Formation; Ward et al. 1991) to central western Florida (Pinecrest Beds; Campbell 1993) and occurs over the same area in the Pleistocene (Ward and Blackwelder 1987; Campbell 1993). Abbott and Morris (1995) gave the modern range as from Brazil to Virginia, but Nicol (1953) considered the northern limit of *G. americana* (and indeed of *Glycymeris* in the western North Atlantic) to be Cape Hatteras (North Carolina; Fig. 2). The latter view is taken in the World Register of Marine Species (WoRMS, undated) and we have seen no evidence in the form of museum specimens or described individuals to contradict it; Abbott and Morris (1995) seem likely to have been mistakenly referring to Pliocene or Pleistocene material from Virginia in their description of the modern range. While *G. americana* occupies much the same geographic range at present as it did in the past, Nicol (1953) noted that it now occurs more patchily and in lower numbers, less commonly reaches a large size, and exhibits a smaller range of morphological variation—indications, in his view, that the species is nearing extinction.

Both ancient and modern forms of *G. americana* are largely restricted to relatively coarse sediments representing current-swept settings (Thomas 1975). They sometimes show evidence of

attack by predators in the form of repair scars and drill holes (Thomas 1976; Sime and Kelly 2016), but drill holes are less frequent in large individuals (B. Kelly, personal communication 2019), suggesting the existence of a size refuge from predation. Large individuals (anterior–posterior length > 70 mm) occur in the Pliocene and are also present in the early Pleistocene (e.g., Fig. 1: JC3, JC4, BC1), with many specimens of this size in early Pleistocene populations from Florida and North Carolina and individuals over 100 mm in length from both states. Apparently referring to modern forms, Abbott and Morris (1995) recorded a length of '5 in.' (127 mm) in the southern part of the range. While we did not observe modern specimens of this great size in our examination of collections at the Natural History Museum, London (BMNH), U.S. National Museum of Natural History, Washington (USNM), and Florida Museum of Natural History, University of Florida, Gainesville (UF), many individuals from Florida are large (e.g., Fig. 1: FL2). Abbott and Morris (1995) stated that *G. americana* is about '½ in.' (13 mm) in length in the northern part of its range, again apparently referring to modern forms. Most of the 90+ dredged valves (45+ individuals) at the USNM from the northernmost part of the modern range (North Carolina) are larger than this, but we discovered amongst these only eight valves (five individuals) exceeding 37 mm in length, with the largest 55 mm in length (Fig. 1: NC2). This information supports the notion of a northward decline in maximum size amongst modern forms, albeit less steep than indicated by Abbott and Morris (1995). The notion is, however, undermined by evidence from a substantial collection of dredged specimens from North Carolina at the North Carolina Museum of Natural Sciences, Raleigh (NCSM). This material, of which we only became aware at a very late stage in our investigation (long after isotopic and growth-increment research had been conducted on a set of specimens from other museums), includes a few valves about 90 mm in length (measurements from photographs kindly supplied by A.E. Bogan, NCSM). The maximum size of modern forms from Florida and North Carolina is therefore similar, although large forms are clearly less common in the latter area. From the evidence of museum collections the species seems to be fairly frequent in North Carolina at present (or at least it was in the mid-twentieth century, when most modern material was obtained) and not obviously

less common than in Florida. However, we discovered very few modern examples from South Carolina and Georgia, evincing the view of Nicol (1953) that the overall abundance of *G. americana* is in decline and perhaps supporting his idea that the species is approaching extinction.

MATERIAL

For the purposes of our investigation we selected four modern specimens (Fig.1, Table 1) and four early Pleistocene specimens (Fig. 1, Table 2) for study, two from Florida and two from North Carolina in each case to allow assessment of latitudinal effects. The geographic provenance of the specimens is shown in Figure 2.

The fossil shells were in a similar condition to the modern ones, being hard, minimally abraded and little perforated by bore holes (Fig. 1). All are from arenaceous units and therefore likely to be from fairly shallow marine settings. Ward and Blackwelder (1987) estimated a depth of 20 m or a little more for the James City Formation (JC3, JC4) while DuBar (1974) estimated a depth of less than 15 m for the Bermont Formation (possible horizon of BC1).

METHODS

All the shells not supplied as 'thick sections' (i.e., all but FL1) were initially photographed. Of these, all but NC1 (see below) were then stabilised by mounting in resin (Buehler EpoThin 2). The mounted shells were then sawn (Buehler Isomet Precision rock saw; 100 rpm) along the line of maximum growth (= dorso-ventral axis) and along parallel lines about 10 mm either side to produce convenient thick sections for growth increment study and isotopic sampling. The faces corresponding to the dorso-ventral axis of each pair of sections were progressively smoothed on a Buehler Metaserve grinder using disks with 600-, 1200- and finally 2500-grit silicon carbide coatings, and then hand-polished using a 0.05 μm aluminium oxide suspension to produce a reflective finish. One of the polished faces was used for growth increment study by standard acetate peel (Richardson and Walker 1993), then by acetate peel after staining the face with Alizarin Red (Johnson et al. 2021),

and finally (following repolishing) by treatment of the face with Mutvei's solution (*c.* 15 minutes immersion; cf. Schöne et al. 2005). Acetate peels were not produced from BC1 because of the limited support from resin on the exterior side. For detailed examination, peels and faces were photographed under a Keyence VHX-7000 digital microscope using High Dynamic Range (HDR) imaging. The non-treated polished face of each pair was also used for growth increment study (likewise with the aid of HDR imaging) and as the preferred source of information (see 'Results and Comparisons') on the number and size of hinge increments. Their width was determined with the custom-made software Panopea (© Peinl and Schöne, 2004) along the line of maximum growth, as illustrated in Johnson et al. (2021). The main part of the shell in the non-treated polished section was drilled for isotope samples under a binocular optical microscope using a fixed drill fitted with a 0.3 mm conical bit, the section being hand-held during the process and brushed to remove any remaining powder after transfer of each sample to a vial for storage. A series of holes *c.* 0.5 mm deep was drilled along a curved path in the outer shell layer, starting as near to the origin of growth (dorsal) as the thickness of the outer layer would permit and proceeding through ontogeny with roughly constant spacing in most cases (Fig. 1: FL1), though with wider spacing in early ontogeny for NC1 (see Fig. 6) and JC3. Mean spacing of the centres of sample holes was from 0.55 mm (NC2) – 0.71 mm (JC3). The smaller specimens were drilled to the ventral margin and the larger (FL2, JC3, JC4, BC1) to a height (measured from the origin of growth by the method of Johnson et al. 2022) of 52.90 mm (JC3) – 58.57 mm (JC4).

Mounting and sectioning of specimens involves an investment of resources and time, and results in permanent disfigurement. Permission for preparation of already-curated specimens in this way is sometimes difficult to obtain, it being seen as prejudicial to other uses—e.g., in studies of morphological evolution. We therefore decided to investigate whether sampling of the shell exterior, as conducted on some modern *Glycymeris* shells with minimal disfigurement and excellent results (e.g., Peharda et al. 2019a) could yield similar results from fossil material. Accordingly, after removal of any surficial organic material through the method adopted by Valentine et al. (2011), the

exterior of specimen NA1 was sampled by drilling sequential commarginal grooves, *c*. 0.1 mm in depth (i.e., within the outer layer) and *c.* 10 mm in length (to obtain sufficient material for possible replicate analysis), straddling the line of maximum growth. The same equipment was used as for sampling cross-sections, the specimen was likewise hand-held, and sample spacing was similar (mean spacing of the centres of grooves: 0.78 mm). A photograph of NA1 seen from the anterior was used for measurement of sample heights from the origin of growth, the last sample being at 54.31 mm, a little short of the ventral margin at 58.48 mm. Sampling from the exterior enabled accurate documentation of the position of sample sites relative to external growth bands and lines (Fig. 1: NA1). In the case of other shells (mounted in resin, sectioned, and sampled in the cut face) the positions of external growth lines (= growth breaks) were determined as well as possible (beneath the encasing resin) and then projected into the sample path in accordance with the orientation of growth structures in the cut face. The sometimes poor definition of these structures, together with the only approximate determination of growth line positions on the exterior, provides scope for error in the location of growth breaks relative to the isotope record in internally sampled shells.

Aliquots of samples (typically 50–100 μg) were analysed for their stable carbon and oxygen isotope composition (given as $\delta^{13}C$ and $\delta^{18}O$ values) at the stable isotope facility, British Geological Survey, Keyworth, UK (NC1, FL1, JC3 *pars*, JC4 *pars*, BC1 *pars*) and the Institute of Geosciences, University of Mainz, Germany (NC2, FL2, JC3 *pars*, JC4 *pars*, NA1, BC1 *pars*). At Keyworth, samples were analysed using an Isoprime dual inlet mass spectrometer coupled to a Multiprep system; powder samples were dissolved with concentrated phosphoric acid in borosilicate Wheaton vials at 90°C. At Mainz, samples were analysed using a Thermo Finnigan MAT 253 continuous flow–isotope ratio mass spectrometer coupled to a Gasbench II; powder samples were dissolved with water-free phosphoric acid in helium-flushed borosilicate exetainers at 72°C. Both laboratories calculated $\delta^{13}C$ and $\delta^{18}O$ against VPDB and calibrated data against NBS-19 (preferred values: +1.95‰ for $\delta^{13}C$, –2.20‰ for $\delta^{18}O$) and their own Carrara Marble standards (Keyworth: +2.00‰ for $\delta^{13}C$, –1.73‰ for $\delta^{18}O$; Mainz: +2.01‰ for $\delta^{13}C$, –1.91‰ for $\delta^{18}O$). Values

were consistently within ± 0.05‰ of the values for $\delta^{18}O$ and $\delta^{13}C$ in NBS-19. This, together with the similarity of seasonal values and continuation of trends in shells analysed partly at Keyworth and partly at Mainz (see the graphs in the online Supplemental Information), confirms the comparability of results from each laboratory established in earlier work (Johnson et al. 2019). Note that $\delta^{18}O$ of shell aragonite was not corrected for different acid-fractionation factors of the aragonite samples and calcite standards (for further explanation see Füllenbach et al. 2015).

We investigated isotopic incorporation by comparing directly measured temperatures at the sites of origin of the modern shells with temperatures calculated from shell $\delta^{18}O$ using the equilibrium equation of Grossman and Ku (1986):

$$T\ (°C) = 20.60 - 4.34*(\delta^{18}O_{arag} - \delta^{18}O_w) \quad (1)$$

and the non-equilibrium equation of Royer et al. (2013):

$$T\ (°C) = 18.11 - 2.66*(\delta^{18}O_{arag} - \delta^{18}O_w) \quad (2)$$

where $\delta^{18}O_{arag}$ is the oxygen isotope ratio of aragonite relative to VPDB (Vienna PeeDee Belemnite) and $\delta^{18}O_w$ is the oxygen isotope ratio of water relative to VSMOW (Vienna Standard Mean Ocean Water). To compensate for measurement against two different scales, 0.27‰ was subtracted from the $\delta^{18}O_w$ value (Gonfiantini et al. 1995). For the $\delta^{18}O_w$ term we used annual mean seafloor values of +0.79‰ (NC1), +0.93‰ (NC2) and +0.94‰ (FL1, FL2), obtained from the gridded data product compiled by LeGrande and Schmidt (2006), which integrates 50 years of observational data and uses high-resolution salinity data and the statistical relationship between $\delta^{18}O_w$ and salinity measurements to fill in missing values. The data are at 1° resolution in latitude and longitude, and are available for every 10 m of depth. Measured temperature (and salinity) data were obtained from decadal averaged monthly mean climatological data from the World Ocean Atlas 2018 (Locarnini et al. 2018; Zweng et al. 2018). These data are obtained from climatological averages based on high-resolution 1955–2017 data, and are at 0.25° resolution in latitude and longitude, and 5 m resolution in depth. The time interval covers the collection period of NC1 and FL1, and possibly FL2. While NC2 was collected prior to the time interval (1913), we verified that there was not a statistically significant shift in

temperature seasonality between the early and mid-20th century in the collection vicinity using outputs from the COBE SST product (Ishii et al. 2005). All the $\delta^{18}O_w$, temperature and salinity data should be interpreted as reflecting long-term climatological values in the vicinity of our collection localities.

For calculation of temperatures from the early Pleistocene shells we used the favoured equation from the investigation of modern shells (see 'Results and Comparisons') together with the lowest and highest modelled $\delta^{18}O_w$ values for the Pliocene of the US eastern seaboard (+0.70‰ and +1.10‰; Williams et al. 2009), there being no modelled values for the early Pleistocene. For the early and late Pliocene, respectively, the modelling produced values of +0.70‰ and +1.10‰ for the North Carolina area, and +0.90‰ and +1.02‰ for the Florida area—i.e., in the early Pliocene a slightly lower value for the former area than the latter (as recorded now; see above), but in the late Pliocene a slightly higher value. From this evidence it seems unlikely that there were significant differences in $\delta^{18}O_w$ between the areas in the early Pleistocene, and the two values chosen for calculation of temperatures represent the minimum and maximum that are likely to have obtained.

The modern temperature and salinity data, together with the isotopic and increment data from shells and the temperatures calculated from $\delta^{18}O$, are provided in the online Supplemental Material.

RESULTS AND COMPARISONS

Growth Structures and Ages

With the exception of NC1, all shells showed some commarginal light/dark banding on the exterior, and amongst these all but JC4 showed prominent growth lines (commarginal steps or indentations in the shell corresponding to growth breaks) at ventral-ward transitions from light to dark shell material (e.g., Fig. 1: NA1); a few such growth lines were also evident at other positions.

In untreated cross-sections, light and dark bands were visible to the naked eye, both in the hinge plate and main part of the shell. However, the bands were not always easily discernible through the

entirety of each, being for instance only evident in the hinge plate of FL2 in the dorsal sector, and in the main part of other large shells generally only well-defined above a height of about 60 mm; in that height range they were observed to be relatively narrow (and composed of dark material bounded by light lines) compared to the less distinct bands visible at heights between about 40 and 60 mm. As far as could be determined, the light and dark material visible on the exterior was equivalent to the same in cross-sections of the main part of the shell. HDR imaging revealed faint light/dark banding in the ventral sector of the hinge plate of FL2 and, with digital enhancement of contrast, increased the visibility of light/dark hinge banding generally (Figs. 3–5), including the dark-band/light-line variety seen at relatively large hinge sizes (Fig. 5) and at equivalent heights in the main part of the shell. HDR imaging also revealed fine banding in the main part of the shell at heights below about 40 mm (Fig. 6).

With the exception of JC4 (Fig. 7; see Johnson et al. 2021 for illustrations of other specimens from this sample, similarly treated to good effect), staining with Alizarin Red did little to improve the definition of growth bands in the hinge plate, as viewed in acetate peel. With or without staining, bands were scarcely visible at all in peels from NC1, despite their clear visibility in the untreated cross-section (Fig. 3). However, they were more evident in peels from other specimens and clear in the dorsal part of the hinge in FL2, although even in this case only a little more so than in the untreated cross-section (Fig. 3). The hinge-bands seen in peels were sharply defined by lines (variably light or dark), whereas those seen in untreated cross-sections had gradational boundaries, a light/dark pair being equivalent to a single band seen in peel (Fig. 3: FL2). The narrow bands seen above a height of about 60 mm in the main part of the shell in untreated cross-sections were also represented in peels (Fig. 7), the dark lines between bands in peels corresponding to the light lines bounding dark bands in untreated cross-sections. Also seen in peels were the wider but less distinct bands at heights between about 40 and 60 mm and the fine bands at heights below about 40 mm (Fig. 7), though the latter were less evident than in untreated cross-sections (Fig. 6). From oxygen isotope evidence that the 31-mm-high specimen in Figure 6 is 5 years old (see Fig. 9: NC1), it is clear that

287 the fine banding at heights below about 40 mm must represent a sub-annual (perhaps tidal)
288 periodicity, whereas the banding at greater shell heights is probably annual, the passage from
289 relatively wide bands at heights between about 40 and 60 mm to narrow thereafter reflecting the
290 ontogenetic slowing of growth typical of bivalves.

291 Treatment of bivalve cross-sections with Mutvei's solution usually enhances the visibility of
292 growth increments (of all scales), these being bounded by sharp ridges of material resistant to the
293 action of the acetic-acid component of the solution (Schöne et al. 2005). None of our specimens
294 responded in this way, although we had some success with other *G. americana* shells. In the hinge
295 plate of our specimens, Mutvei's solution gave a pale blue colour to the bands of light material but
296 did not make them any more distinct from dark bands (Figs. 3, 4). In the main part of the shell,
297 treatment with the solution sometimes produced zones of stronger and weaker blue coloration, with
298 the number of the former the same as that of dark bands in the hinge plate in one case (Fig. 3: NC1).
299 However, in other cases zonation was either not produced (Fig. 3: FL2) or was not relatable to the
300 banding in the hinge plate (Fig. 4).

301 The most clearly and consistently visualised growth structure in our *G. americana* specimens was
302 the light/dark banding of untreated hinge cross-sections, as seen in HDR images with enhanced
303 contrast. In so far as this banding is apparently equivalent to the banding seen (usually) in peels, and
304 hinge bands in peels from *G. glycymeris* have been shown to represent annual increments (Brocas et
305 al. 2013), the light/dark hinge banding in our specimens can be used to supply estimates of age in
306 years. We interpreted some relatively narrow bands of dark material within light, and of light
307 material within dark, as adventitious (perhaps due to passing encounters with predators or mild
308 fishing disturbance; Ramsay et al. 2000), basing our definition of annual increments in these cases on
309 the broader light and dark bands in which the narrow bands were included. However, even where
310 very narrow, we took the first dark band as the complement of the preceding light one (i.e., the two
311 as an annual pair) because to have done otherwise would have led to identification of an improbably
312 large first annual increment. Our approach is illustrated in Figures 3–5 and the resultant age

estimates are given in Table 3. Included in the table is an estimate for the unsectioned specimen NA1 based on the external light/dark banding of the main part of the shell (Fig. 1), given that this appears to correspond to the light/dark banding seen in cross-section, which is probably annual.

From hinge-banding evidence, the smaller of the two modern North Carolina shells (NC1; length 37 mm) was 4 years old when it died, the larger (NC2; length 55 mm) 9 years old, and the smaller of the two modern Florida shells (FL1; length 74 mm) 10 years old. The larger of the modern Florida shells (FL2; length 91 mm) shows 6 bands in the first half of hinge ontogeny but equivalent structures cannot be clearly seen thereafter. At least the same amount of time is likely to be represented by the second half of hinge ontogeny because growth typically declines with age in bivalves, so we can infer a minimum age at death of 12 years. Modern specimens of similar size are quite common in Florida so we can further infer that this minimum age is reached frequently there. North Carolina specimens of a size greater than the largest investigated from there (NC2; length 55 mm) are relatively rare, so while the age of the latter specimen (apparently 9 years) is no doubt exceeded by some, it is probably not by many—i.e., the age structure of modern *G. americana* populations may well differ between North Carolina and Florida.

Banding evidence suggests long lifespans in early Pleistocene *G. americana* from North Carolina. While JC4 (86 years in this investigation; 89 years in Johnson et al. 2021, as measured by A.C. Featherstone from a peel) appears to be an exceptionally long-lived individual (Johnson et al. 2021), JC3 (31 years in this investigation; 23 years in Johnson et al. 2021, as measured by A.C. Featherstone from a peel) probably represents the other end of the range of 'normal' lifespans, a greater age (42 years) being specified by a very clear peel record from the hinge plate of a larger specimen (length 107 mm) from the same unit and locality (JC1 in Johnson et al. 2021). Specimens the same size or larger than JC3 (length 87 mm) are quite common at this site, as they are also in another early Pleistocene unit (Waccamaw Formation) at a more southerly locality (Clyde Moor Quarry) in North Carolina: a larger specimen than JC3 from there (length 107 mm) supplied a peel-based age of 46 years, a slightly smaller one (length 83 mm) an age of 49 years, and four other

specimens of lengths 71–78 mm ages of 25–46 years (Johnson et al. 2021). While these determinations were by another operative (K.A. Richardson), and different operatives and visualisation methods can provide significantly different figures (see above), ages greater than 20 years were probably achieved quite commonly during the early Pleistocene in North Carolina, in likely contrast to now.

The existing banding evidence does not suggest such long lifespans in Florida as in North Carolina during the early Pleistocene. The larger of the two Florida shells investigated (BC1; length 84 mm) is only fractionally smaller than JC3 but apparently lived only 15 years. The smaller (NA1; length 68 mm) almost certainly died at a younger age because the 6 annual increments recognised in the main shell constitute nearly all of ontogeny, probably no more than 3 further years being represented by earlier and later growth (Fig. 1). However, specimens of much greater size are common in the early Pleistocene of Florida (up to a length of 110 mm in the Nashua Formation; UD 53428) so substantially greater ages are probable, and it may be that old specimens are as common as in the early Pleistocene of North Carolina.

Plots of hinge size against age from hinge increments (Fig. 8A) suggest slower growth in North Carolina than Florida at present and in the early Pleistocene. This conforms with the pattern of poleward decrease in growth rate seen in other bivalves (Moss et al. 2016) but requires confirmation from investigation of further specimens (see also 'Oxygen Isotopes, Ages, Growth Rates and Temperatures' for discussion of relative growth rates from plots of shell height against age from oxygen isotope cycles).

Oxygen Isotopes, Ages, Growth Rates and Temperatures

All the $\delta^{18}O$ profiles (Fig. 9) show the anticipated cyclicality, reflecting seasonal differences in water temperature (low $\delta^{18}O$ values representing the warm temperatures of summer, high $\delta^{18}O$ values the cool temperatures of winter). The cyclicality is smoothest and most regular in the externally sampled shell (NA1) and corresponds precisely with the light/dark banding seen on the exterior, high

values falling in dark bands. The assumption that this banding can be used to determine age (see 'Growth Structures and Ages') is therefore shown to be valid.

The ages indicated by the number of $\delta^{18}O$ cycles are given in Table 3. The 8 cycles from FL2 fall within the first 53 mm of shell height. The summer-to-summer wavelength of the last cycle is 8 mm so conservatively assuming the same wavelength for the rest of ontogeny a total of 11 cycles would have been identified if sampling had continued to the ventral edge (height 81 mm). Projecting the number of increments to the end of hinge ontogeny gave almost the same figure (12) but both are probably underestimates of the number of years that the animal lived because of the typical ontogenetic decline in growth rate. The 9 $\delta^{18}O$ cycles from JC3, 19 from JC4, 8 from NA1 and 8 from BC1 also fall within only a part of shell ontogeny as measured by height: the first 53 mm of 82 mm, 59 mm of 82 mm, 54 mm of 58 mm and 53 mm of 76 mm, respectively. By the method applied to FL2, if sampling had been continued to the ventral edge, total lifespans of 16, 38, 9 and 13 years, respectively, would have been identified. Again, these figures are very likely underestimates of the age at death, especially in the case of the large shells JC3 and JC4, so the large discrepancies with the ages indicated by hinge-banding for JC3 and JC4 are unsurprising. For all the other shells the ages determined or projected from $\delta^{18}O$ evidence are within 2 years of those inferred from banding evidence, and the ages of the modern shells sampled to the ventral margin (NC1, NC2, FL1) are within 1 year of those determined from banding evidence (Table 3). This shows that band-counting is a quite accurate means of determining age in *G. americana*, subject to use of an effective technique (e.g., HDR imaging) to enhance the visibility of annual bands. Plots of shell height against age as determined from $\delta^{18}O$ cycles (Fig. 8B) provide some indication of the geographic difference in growth rates inferred from plots of hinge height against age from hinge increments (Fig. 8A). However, the evidence of slower growth in North Carolina is weaker, especially when account is taken of the fact that the apparently very slow-growing early Pleistocene specimen JC4 is unusually thick-shelled—i.e., while it certainly grew very slowly in terms of shell height, the rate at which it secreted carbonate may well have been similar to that of other individuals (Johnson et al. 2021).

For the three modern shells sampled to the ventral edge we can use the $\delta^{18}O$ profile to determine the season of death. In all three the last segment comprises falling values, so death occurred in spring (NC2, FL1) or summer (NC1), before the date of collection in each case (Table 1).

The right-hand plots in Figure 10 show temperature profiles calculated from the shell $\delta^{18}O$ values of each of the modern specimens, while the left-hand plots show measured monthly temperature and salinity data (in practical salinity units; PSU) for the locations concerned. The limited variation in seafloor salinity and low correlation (see *r* values) with seafloor temperature at the locations of NC1, NC2 and FL1 suggest that the calculated temperature profiles are unlikely to be distorted by use of a single (annual mean) water $\delta^{18}O$ value in each of these cases. The greater variation in seafloor salinity at the location of FL2 and higher (negative) correlation with seafloor temperature suggest that here, winter and summer water $\delta^{18}O$ values may be less well represented by the annual mean and that the calculated temperature profile may be somewhat distorted due to the interaction with changing water $\delta^{18}O$ values (artificially low winter temperatures and high summer temperatures).

A comparison of calculated winter minimum and summer maximum temperatures from the modern shells with the measured values at their locations (Fig. 10) shows the close approximation to reality of temperatures obtained with the equation of Grossman and Ku (1986) and the significant departure from reality of the temperatures obtained using the equation of Royer et al. (2013). The latter gives underestimates of both winter and summer temperatures but especially of the latter, resulting in an underestimate also of seasonal range. Such discrepancies as exist between measured seasonal temperatures and those calculated using the equation of Grossman and Ku (1986) could reflect differences in the years represented (i.e., inter-annual variation in seasonal extremes). Recalculating the 'Grossman and Ku' temperature profile from FL2 with salinity-adjusted values for water $\delta^{18}O$ would have the effect of raising winter temperatures and lowering summer temperatures, assuming a normal (positive) relationship between salinity and water $\delta^{18}O$. While this would increase the discrepancy with measured winter and summer temperatures, it would do so very little due to the variation of only 1.26 PSU between winter (March) and summer (October) salinity. On the basis of

typical salinity/water $\delta^{18}O$ relationships (e.g., Harwood et al. 2008), this variation would alter calculated winter and summer temperatures by less than 1°C, leaving discrepancies with measured temperatures well within the range plausibly accountable to inter-annual variation in seasonal extremes.

The shape of the temperature profiles from most shells (cuspate winter sectors, rounded summer sectors) is indicative of a decline in growth during the coldest part of the year. In so far as the calculated winter minimum temperatures (using the equation of Grossman and Ku 1986) are close to measured values it appears that sampling was at a sufficiently high resolution to avoid significant time-averaging and misrepresentation of the minimum temperatures experienced. The paucity of growth breaks associated with winter temperature minima is a factor that might have contributed to the closeness of the isotope-derived and measured winter values. However, growth breaks are commonly associated with summer temperature maxima (see NC2 and FL1), yet the isotope-derived and measured summer values are as close as the corresponding winter values. From this, and the fact that isotope-derived temperatures in summers without growth breaks are essentially the same as those in summers with them (again, see NC2 and FL1), one is led to the conclusion that growth breaks were of short duration, representing significant cases of such brief events as predator attack or fishing disturbance (Ramsay et al. 2000), and their presence or absence thus has little influence on the fidelity of the isotope-derived temperature record to reality.

Figure 11 shows temperature profiles for the fossil shells calculated using the evidently superior equation of Grossman and Ku (1986) and the maximum and minimum plausible values for water $\delta^{18}O$ inferred herein. Growth breaks are relatively rarely associated with seasonal temperature extremes, and where there is a correspondence it is usually with winter extremes, unlike in the modern shells. The first two growth breaks (heights 14.9 and 22.7 mm) in JC3 are associated with much warmer winter extremes than are registered in some later years without winter growth breaks, the higher temperatures presumably reflecting sufficiently long interruptions of growth for significant truncation of the record. In each of NA1 and BC1, however, the first growth break

(heights 15.5 and 26.4 mm, respectively) is associated with a winter extreme much like those registered in later years without winter growth breaks. The duration of these growth breaks was therefore presumably short and the impact on the isotopic temperature record minimal, as inferred for all growth breaks in modern shells. It is worth noting that in NA1, the shell in which the position of growth breaks was most reliably determined, their location in the temperature profile is mainly in intervals of declining temperature. Such fall growth breaks are known in other bivalve taxa (e.g., *Arctica islandica*; Schöne 2013) and it may be that the summer and winter growth breaks recorded in some of our *G. americana* shells (fossil and modern) are actually examples of these, misidentified as a result of inaccurate determination of their positions (see 'Methods'). If so, they can have had no influence on the seasonal temperature extremes registered. In comparison to other fossil shells, the profile from JC4 has a noticeably lower amplitude and wavelength. The latter parameter indicates slow extensional growth in this specimen (confirming the increment-based interpretation of Johnson et al. 2021), which would have caused time-averaging in sampling and hence the reduced amplitude. Amplitude and wavelength are particularly low over the last 5 years represented, manifesting the ontogenetic slowing of growth typical of bivalves. In view of these observations the profile from JC4 must be taken as a truncated record of seasonal temperature variation. However, it seems reasonable to view the profiles from the three other fossil shells as accurate indicators of seasonal temperature range on the seafloor. There is no reason to think that external sampling of NA1 had any effect on the range recorded, as it is very similar to that from the other early Pleistocene shell from Florida (BC1), sampled internally. It is striking that all three shells show ranges in some (JC3, BC1) or all (NA1) years that are somewhat larger than the modern average seafloor range in the relevant state (Fig. 11). While this might reflect relatively shallow situations or chance sampling of intervals with relatively high seasonality, higher seasonality than now is also indicated by early Pleistocene examples of the scallop *Carolinapecten eboreus* from Florida and North Carolina (Johnson et al. 2019, table 3), including two specimens (EPLE-MACP 11 and 12) from the same unit and locality as JC3. Like results from *C. eboreus*, those from *G. americana* specimens JC3, NA1 and BC1 suggest

469 that increased seasonality was largely a consequence of cooler winters than now, rather than warmer
470 summers, and some cooler winters are even shown by the truncated record from JC4 (Fig. 11). While
471 this conclusion (the same as that of Ivany et al. 2000 for the Eocene/Oligocene transition in the Gulf
472 Coastal Plain) is dependent on assumed values for water $\delta^{18}O$, it is very credible because cooler
473 winters are indicated using not only the minimum but also the maximum plausible value inferred
474 herein (giving warmer temperatures for a given shell $\delta^{18}O$), and this value (+1.10‰) is higher than
475 the present water $\delta^{18}O$ value in both Florida and North Carolina (see 'Methods'). Maximum and
476 minimum temperatures at the surface are likely to have been slightly warmer and cooler,
477 respectively, than on the seafloor (cf. Fig. 10, left-hand diagrams), thus the surface range would have
478 been still larger than the seafloor range. While seasonality appears from this evidence to have been
479 greater in the early Pleistocene, the latitudinal temperature gradient was evidently as low as at
480 present, there being little difference between the summer temperatures from the *G. americana* shells
481 from Florida and North Carolina (excluding JC4), and likewise between the winter temperatures, just
482 as between modern measured temperatures at comparable latitudes (Figs. 10, 11).
483 Figure 12 pools and summarises the seasonal temperature data (calculated with the equation of
484 Grossman and Ku 1986) from the early Pleistocene and modern shells of Florida and North Carolina,
485 but excluding JC4 for the reasons given above. Unsurprisingly, in view of the excellent match
486 between calculated and measured temperatures at each of the individual locations concerned, the
487 pooled data from the modern shells accurately depict the low latitudinal temperature gradient
488 between Florida and North Carolina shown by measured values (Figs. 10, 11). Likewise
489 unsurprisingly, the pooled data from the early Pleistocene shells bear out the impression gained from
490 consideration of individual profiles that the latitudinal temperature gradient was similarly low at that
491 time. However, only the data from Florida bear out the impression of greater seasonality than now,
492 and by cooler winters alone just in the case of temperatures calculated using a water $\delta^{18}O$ value of
493 +0.70‰. This is a result of pooling data from all years and might be seen as a more realistic picture
494 than that gained from consideration of individual profiles and the years within them showing greatest

seasonal variation. However, it must be remembered that the data for North Carolina are solely from JC3 and include two high winter values that are almost certainly substantial overestimates as a result of growth cessation. Exclusion of these and inclusion of winter values from JC4 (which would be reasonable because even the lowest are also almost certainly overestimates) would give a more convincing picture of greater seasonality, caused by somewhat cooler winters.

Carbon Isotopes

With the exception of fossil specimen BC1 (+0.01 ± 0.96‰; ± 1σ), the mean $\delta^{13}C$ values from the modern and fossil shells, calculated from the data in Figure 9, lie in small, very similar ranges, between +1.84 ± 0.25‰ (NC1) and +2.33 ± 0.20‰ (NC2) for the former and between +1.78 ± 0.25‰ (JC4) and +2.32 ± 0.29‰ (NA1) for the latter. These values are a little lower than those (+2.42 ± 0.40‰, +2.69 ± 0.32‰) from two fossil (late Pliocene) specimens of *G. radiolyrata* from Belgium (Johnson et al. 2022). As in *G. radiolyrata*, the $\delta^{13}C$ profiles from *G. americana* show cyclicality, with an amplitude lower (again excepting BC1) but a wavelength similar to that of $\delta^{18}O$ (i.e. the variation is seasonal), although typically with an in-phase rather than antiphase relationship. This relationship is expressed by generally positive (albeit small) correlation coefficients for entire $\delta^{13}C$ and $\delta^{18}O$ datasets (see Fig. 9) but is more readily appreciated in the form of short-term parallel trends in the variables (e.g. the successive parallel increases and decreases shown by NA1; Fig. 9). Seasonal variation in $\delta^{13}C$ has been documented by Gillikin et al. (2007) in Pliocene and modern *Mercenaria mercenaria* and by Chauvaud et al. (2011) in modern *Pecten maximus*. The latter authors attributed the pattern to variation in food availability, leading to corresponding variation in the contribution of dietary/metabolic carbon (isotopically light) to shell carbon. However, the $\delta^{13}C$ value of dissolved organic carbon (e.g., as determined by phytoplankton photosynthesis) also influences shell $\delta^{13}C$ in *P. maximus* (Marchais et al. 2015) and seasonal variation in this parameter has been said to be the cause of seasonal variation in $\delta^{13}C$ in other bivalves (e.g., Arthur et al. 1983; Krantz et al., 1987, 1988).

DISCUSSION

Differences in Age Structure of Populations

There is a strong suggestion that modern populations of *G. americana* from North Carolina include fewer old individuals than modern populations from Florida, and rather firmer evidence that they include fewer old individuals than early Pleistocene populations from North Carolina. The apparent reduction in frequency of old individuals over time in North Carolina could reflect increased predation in view of the evidence of somewhat warmer conditions now and the usual positive relation between predation intensity and temperature (Vermeij 1987). However, there are no direct indications of an early Pleistocene–present increase in predation in North Carolina, and the probably higher present-day frequency of old forms in Florida (slightly warmer) argues against any control of age structure by predation.

Human harvesting of large, relatively old individuals for food has been implicated in Holocene changes of age structure in *Crassostrea virginica* populations of the U.S. eastern seaboard (Lockwood and Mann 2019; Hesterberg et al. 2020). However, this is not an explanation applicable to the early Pleistocene–present decline in the frequency of old *G. americana* individuals in North Carolina because this species is neither now, nor ever has been, thus exploited in the region. Removal of large *G. americana* individuals in the process of harvesting other species certainly has occurred, as shown by the existence of such specimens in museum collections from the Cape Canaveral (Florida) area that were either obtained live in the process of scallop trawling (e.g., USNM 821429) or recovered from waste heaps of scallop shells (e.g., BMNH 20094595). The scallop species harvested there, *Argopecten gibbus* (calico scallop), has also been exploited intermittently since 1959 in North Carolina (Cummins 1971), with a by-catch including *G. americana* (Porter and Wolfe 1971). None of the 20 individuals (40 paired valves; USNM 765105, 76106, 76110) of *G. americana* dredged live or recently-dead off Ocracoke Inlet by the survey vessel ‘Silver Bay’ in 1961

(i.e., shortly after the start of scallop exploitation in North Carolina) has a length greater than 37 mm, whereas of the few large (length *c*. 90 mm) modern individuals from North Carolina that became known to us late in our investigation, one (NCSM 10680) was collected in 1949 and another (NCSM 7844) in 1951 (i.e., both before the start of scallop exploitation). While these data are consistent with the notion that the modern paucity of large *G. americana* in North Carolina is due to scallop trawling (causing their removal or perhaps the early death of individuals by disturbance or damage), the high frequency of large (presumably old) modern forms from Florida, where scallop trawling has also occurred since 1959, and on a larger scale (Blake and Moyer 1991), suggests that this is not an influence on the age structure of populations. It may be that many of the large modern Florida specimens were collected before 1959, or that they were actually obtained through scallop harvesting. However, until this is shown, it is appropriate to consider other explanations for differences in age structure, particularly the most firmly established difference between early Pleistocene and modern populations in North Carolina. One possibility is that the high frequency of old forms there in the early Pleistocene is a reflection of the isotopically-demonstrated relatively cool conditions; such circumstances are conducive to longer life in bivalves (Moss et al. 2016). Another more speculative possibility is that there was local continuation into the Pleistocene of the high productivity conditions that existed more widely at earlier times on the U.S. eastern seaboard (Riggs 1984; Allmon 2001; Anderson 2001; Johnson et al. 2019), and that this favoured longer life. High productivity is, however, associated with faster growth rather than longer life in the co-occurring bivalve *Carolinapecten eboreus* (Johnson et al. 2019). Further investigation of these possible non-anthropogenic controls on age structure would illuminate the amount of future bottom-trawling permissible without jeopardizing the survival of benthic species.

Early Pleistocene Marine Climate and Oceanography of the U.S. Eastern Seaboard

We have shown that, subject to the accuracy of our chosen water $\delta^{18}O$ values, winter seafloor temperatures in the early Pleistocene were a little lower than now in both Florida and North Carolina.

573 The early Pleistocene winter temperatures from *G. americana* are still in the subtropical range but
574 there are indications of lower temperatures from *C. eboreus*—into the cool temperate winter range in
575 North Carolina (Johnson et al. 2019). Since the values from North Carolina *C. eboreus* include some
576 from the unit and locality (James City Formation, Lee Creek Mine) supplying the North Carolina *G.*
577 *americana* investigated herein, one must presume some short-term fluctuation in winter conditions,
578 but about a mean state cooler than the present winter temperature. Early Pleistocene summer
579 temperatures were seemingly at least sometimes as high as at present in Florida and North Carolina
580 so it is difficult to interpret the cooler winters than now in terms of global change to the icehouse
581 conditions of the later Pleistocene. Rather, they seem more likely to reflect a fairly continuous and
582 large supply of cool water from the north beyond the latitude of Cape Hatteras, in contrast to the
583 situation on the shelf now but as proposed for the Pliocene to account for low winter temperatures in
584 southern North Carolina (Johnson et al. 2017). Such a supply, equivalent to that at present in the
585 western South Atlantic transporting high-latitude waters to the shelf as near the equator as 23°S
586 (Bisbal 1995), would bring nutrients (Johnson et al. 2017), thereby enhancing primary production
587 and conceivably providing the means for more *G. americana* individuals to reach a substantial age
588 (see 'Differences in Age Structure of Populations'). Intermittent present-day 'leakage' of northern
589 waters along the shelf to latitudes a few degrees south of Cape Hatteras has long been recognised
590 (Pietrafesa et al. 1994) but a more continuous southward flow offshore at depth has now been
591 observed (Andres et al. 2018). Upwelling of such deep water, just as happens in the subtropical
592 western South Atlantic (Castelao et al. 2004), could result in cool shelf conditions south of Cape
593 Hatteras. Presumably this does not happen much now—summer temperatures are high south and
594 (some way north) of Cape Hatteras, and winter temperatures are much higher south than north of this
595 feature (Johnson et al. 2017)—but it might have done in the early Pleistocene if the Gulf Stream
596 (which flows north along the shelf edge as far as Cape Hatteras) often occupied a relatively offshore
597 position (cf. Castelao et al. 2004). Occasional switches to a more nearshore position would have cut
598 off this supply and allowed intrusions of warm water onto the shelf (Atkinson 1977; Castelao 2011,

599 Zeng and He 2016), possibly accounting for the higher (but still cool) winter temperatures recorded
600 by *G. americana* compared to *C. eboreus.* At present, Gulf-Stream incursions only have an influence
601 as far as the mid-shelf (Lee et al. 1991), so it is questionable whether they would have affected the
602 shallow-water settings of the early Pleistocene shells discussed herein. However, it is worth noting
603 that in the subtropical western South Atlantic cool-water incursions can extend onto the Brazilian
604 shelf as far as the coast (Castelao et al. 2004).
605
606 ## CONCLUSIONS AND FURTHER WORK
607 The principal conclusions of this work are as follows:
608 (1) *G. americana* precipitates its shell in oxygen isotopic equilibrium with seawater;
609 (2) cyclical $\delta^{18}O$ data, reflecting seasonal temperature variation, can be obtained by serial sampling
610 of the outer shell layer from the exterior as well as in cross-section;
611 (3) the $\delta^{18}O$ data facilitates age determination, both directly (by the annual nature of cycles) and
612 indirectly (by confirming that various forms of growth structure are likewise annual, or very nearly
613 so);
614 (4) interruptions in shell growth are usually brief, enabling accurate reconstruction of seasonal
615 temperature maxima and minima from high resolution $\delta^{18}O$ profiles;
616 (5) $\delta^{18}O$ data from *G. americana* indicate that the temperature gradient between Florida and North
617 Carolina (to the latitude of Cape Hatteras) was as low in the early Pleistocene as now;
618 (6) the seasonal range in temperature was somewhat greater in the early Pleistocene than now in both
619 Florida and North Carolina, due to lower winter temperatures;
620 (7) lower winter temperatures in the early Pleistocene may have been due to greater and more
621 extensive supply of cool northern waters to latitudes south of modern Cape Hatteras, with shelf
622 transport supplemented by upwelling of water brought south at depth;
623 (8) modern populations of *G. americana* from North Carolina do not lack large individuals (contrary
624 to the view of Abbott and Morris 1995) but they are rare, so these populations probably include

625 fewer old individuals than modern populations from Florida and (more definitely) early Pleistocene
626 populations from North Carolina;
627 (9) the temporal change in age structure of *G. americana* populations in North Carolina may be an
628 effect of recent scallop fishing but could be a result of earlier (non-anthropogenic) environmental
629 changes.
630 It would be valuable to test the early Pleistocene temperature results presented herein with
631 independent proxy data from the same shells. The two most promising approaches are carbonate
632 clumped isotope (Δ_{47}) analysis and measurement of biomineral unit (BMU) size, shape and
633 orientation. The Δ_{47} approach has been successfully applied to various modern and fossil bivalves
634 (e.g., Douglas et al. 2014; Briard et al. 2020; Caldarescu et al. 2021; de Winter et al., 2022; Huyghe
635 et al. 2022; Wichern et al. 2023; Zhang and Petersen 2023) and the BMU approach likewise (e.g.,
636 Gilbert et al. 2017; Milano et al. 2017a, b; Höche et al. 2021), including to *Glycymeris* (modern
637 examples of *G. bimaculata*; Höche et al. 2020). There is great scope for also applying these
638 approaches, and the $\delta^{18}O$-based approach used herein, to Pliocene *G. americana* of the U.S. eastern
639 seaboard, in particular to investigate the mid-Piacenzian warm period, the most recent interval in
640 Earth history when global temperature was as high as anticipated at the end of this century (Dowsett
641 et al. 2019). It would be for instance possible and useful to test the accuracy and meaning (season
642 represented) of other geochemical and biotic temperature proxies applied in this interval and area
643 (e.g. Dowsett et al. 2021). Investigation of life history using $\delta^{18}O$ and growth increment data could
644 also be extended to Pliocene *G. americana* in order to determine if and how this character evolves in
645 response to climate fluctuations (Moss et al. 2021).
646
647 ACKNOWLEDGMENTS
648 We thank Roger Portell and John Slapcinsky (Florida Museum of Natural History), and Ellen
649 Strong (U.S. National Museum of Natural History), for loaning specimens in their care for analysis;
650 Tom White (Natural History Museum, London) for loaning comparative material in his care; Art

651 Bogan (North Carolina Museum of Natural Sciences) for providing photographs of specimens in his
652 care and information on their date of collection; and Rick Luettich (University of North Carolina at
653 Chapel Hill) for tracking down the specimens held at the North Carolina Museum of Natural
654 Sciences. Roger Portell and Buck Ward (Virginia Museum of Natural History) kindly facilitated and
655 guided ALAJ on visits to fossil sites in, respectively, Florida and North Carolina, at which further
656 specimens were obtained for analysis and comparative use. Mark Dean and Matt Hunt (University of
657 Derby) mounted, sectioned, ground and polished shells. Peel-based estimates of the ages of examples
658 from the James City and Waccamaw formations were obtained by Aaron Featherstone and Kathryn
659 Richardson in the context of the Undergraduate Research Scholarship Scheme of the University of
660 Derby (URSS17-028 and URSS17-029). We thank Bridget Kelly (formerly University of North
661 Carolina Wilmington) for permission to refer to unpublished information and Roger Thomas
662 (Franklin & Marshall College) for providing insights into the modern distribution and size of *G.*
663 *americana.* We also express our appreciation to the two reviewers and Associate Editor for their
664 detailed comments on the initial submission, which led to significant improvements in the final
665 version. ALAJ gratefully acknowledges support from the Leverhulme Trust (RPG-2021-090).
666

667 SUPPLEMENTAL MATERIAL

668 Data are available from the PALAIOS Data Archive: [URL to be provided]
669

670 REFERENCES

671 ABBOTT, R.T. AND MORRIS, P.A., 1995 Shells of the Atlantic and Gulf Coasts and the West Indies
672 (4th Edition): Houghton Mifflin, New York, 350 p.
673 ALEXANDROFF, S.J., BUTLER, P.G., HOLLYMAN, P.R., SCHÖNE, B.R. AND SCOURSE, J.D., 2021, Late
674 Holocene seasonal temperature variability of the western Scottish shelf (St Kilda) recorded in
675 fossil shells of the bivalve *Glycymeris glycymeris*, Palaeogeography. Palaeoclimatology,

676 Palaeoecology, v. 562, number 110146 (15 p.), 7.9 MB, doi: 10.1016/j.palaeo.2020.110146.
677 Checked April 2023.
678 ALLMON, W.D., 2001, Nutrients, temperature, disturbance, and evolution: a model for the late
679 Cenozoic marine record of the western Atlantic: Palaeogeography, Palaeoclimatology,
680 Palaeoecology, v. 166, p. 9–26, doi: 10.1016/S0031-0182(00)00199-1.
681 ANDERSON, L.C., 2001, Temporal and geographic size trends in Neogene Corbulidae (Bivalvia) of
682 tropical America: using environmental sensitivity to decipher causes of morphologic trends:
683 Palaeogeography, Palaeoclimatology, Palaeoecology, v. 166, p. 101–120, doi: 10.1016/S0031-
684 0182(00)00204-2.
685 ANDRES, M., MUGLIA, M., BAHR, F., AND BANE, J., 2018, Continuous flow of Upper Labrador Sea
686 Water around Cape Hatteras: Scientific Reports, v. 8, number 4494 (8 p.), 3.0 MB, doi:
687 10.1038/s41598-018-22758-z.
688 ARTHUR, M.A., WILLIAMS, D.F., AND JONES, D.S., 1983, Seasonal temperature-salinity changes and
689 thermocline development in the mid-Atlantic Bight as recorded by the isotopic composition of
690 bivalves: Geology, v. 11, p. 655–659, doi: 10.1130/0091-7613(1983)11<655:STCATD>2.0.CO;2.
691 ATKINSON, L.P., 1977, Modes of Gulf Stream intrusion into the South Atlantic Bight shelf waters:
692 Geophysical Research Letters, v. 4, p. 583–586, doi: 10.1029/GL004i012p00583.
693 BEAVER, P.E., BUCHER, D.J., AND JOANNES-BOYAU, R., 2017, Growth patterns of three bivalve
694 species targeted by the ocean cockle fishery, southern New South Wales: *Eucrassatella kingicola*
695 (Lamarck, 1805); *Glycymeris grayana* (Dunker, 1857); and *Callista* (*Notocallista*) *kingii* (Gray,
696 1827): Molluscan Research, v. 37, p. 104–112, doi: 10.1080/13235818.2016.1253430.
697 BERTHOU, P., BLANCHARD, M., NOEL, P., AND VERGNAUD-GRAZZINI, C., 1986, The analysis of
698 stable isotopes of the shell applied to the determination of the age of four bivalves of the
699 "Normano-Breton" Gulf, Western Channel: International Council for the Exploration of the Sea,
700 Shellfish Committee, v. K16, p. 1–13.

701 BISBAL, G.A., 1995, The Southeast South American shelf large marine ecosystem: evolution and
702 components: Marine Policy, v. 19, p. 21–28, doi: 10.1016/0308-597X(95)925709-W.
703 BLAKE, N.J. AND MOYER, M.A., 1991, The calico scallop, *Argopecten gibbus*, fishery of Cape
704 Canaveral, Florida, *in* S.E. Shumway (ed.), Scallops: Biology, Ecology and Aquaculture
705 (Developments in Aquaculture and Fisheries Science, 21): Elsevier, Amsterdam, Oxford, New
706 York, Tokyo, p. 899–911.
707 BRIARD, J., PUCÉAT, E., VENNIN, E., DAËRONC, M., CHAVAGNAC, V., JAILLET, R., MERLE, D., AND
708 DE RAFÉLIS, M., 2020, Seawater paleotemperature and paleosalinity evolution in neritic
709 environments of the Mediterranean margin: Insights from isotope analysis of bivalve shells,
710 Palaeogeography, Palaeoclimatology, Palaeoecology, v. 543, number 109582, doi:
711 10.1016/j.palaeo.2019.109582.
712 BROCAS, W.M., REYNOLDS, D.J., BUTLER, P.G., RICHARDSON, C.A., SCOURSE, J.D., RIDGWAY, I.D.,
713 AND RAMSAY, K., 2013, The dog cockle, *Glycymeris glycymeris* (L.), a new annually-resolved
714 sclerochronological archive for the Irish Sea: Palaeogeography, Palaeoclimatology, Palaeoecology,
715 v. 373, p. 133–140, doi: 10.1016/j.palaeo.2012.03.030.
716 BUŠELIĆ, I., PEHARDA, M., REYNOLDS, D.J., BUTLER, P.G., ROMÁN GONZÁLEZ, A., EZGETA-BALIĆ,
717 D., VILIBIĆ, I., GRBEC, B., HOLLYMAN, P., AND RICHARDSON, C.A., 2015, *Glycymeris bimaculata*
718 (Poli, 1795)—A new sclerochronological archive for the Mediterranean?: Journal of Sea Research
719 v. 95, p. 139–148, doi: 10.1016/j.seares.2014.07.011.
720 CALDARESCU, D.E., SADATZKI, H., ANDERSSON, C., SCHÄFER, P., FORTUNATO, H., AND MECKLER,
721 A.N., 2021, Clumped isotope thermometry in bivalve shells: A tool for reconstructing seasonal
722 upwelling: Geochimica et Cosmochimica Acta, v. 294, p. 174–191, doi:
723 10.1016/j.gca.2020.11.019.
724 CAMPBELL, L.D., 1993, Pliocene molluscs from the Yorktown and Chowan River formations in
725 Virginia: Commonwealth of Virginia, Virginia Division of Mineral Resources Publication 127,
726 Charlottesville, 259 p.

727 CASTELAO, R., 2011. Intrusions of Gulf Stream waters onto the South Atlantic Bight shelf: Journal of
728 Geophysical Research Oceans: Oceans, v. 116, number C10011, doi: 10.1029/2011JC007178.
729 Checked July 2023.
730 CASTELAO, R.M., CAMPOS, E.J.D., AND MILLER, J.L., 2004, A modelling study of coastal upwelling
731 driven by wind and meanders of the Brazil Current: Journal of Coastal Research, v.20, p. 662–671,
732 doi: 10:2112/1551-5036(2004)20[662:AMSOCU]2.0.CO;2.
733 CHAUVAUD, L., THÉBAULT, J., CLAVIER, J., LORRAIN, A., AND STRAND, Ø., 2011, What's hiding
734 behind ontogenetic $\delta^{13}C$ variations in mollusk shells? New insights from the Great Scallop (*Pecten*
735 *maximus*): Estuaries and Coasts, v. 34, p. 211–220, doi: 10.1007/s12237-010-9267-4.
736 COX, L.R., NEWELL, N.D., BOYD, D.W., BRANSON, C.C., CASEY, R., CHAVAN, A., COOGAN, A.H.,
737 DECHASEAUX, C., FLEMING, C.A., HAAS, F., HERTLEIN, L.G., KAUFFMAN, E.G., KEEN, A.M.,
738 LAROQUE, A., MCALESTER, A.L., MOORE, R.C., NUTTALL, C.P., PERKINS, B.F., PURI, H.S.,
739 SMITH, L.A., SOOT-RYEN, T., STENZEL, H.B., TRUEMAN, E.R., TURNER, R.D., AND WEIR, J., 1969,
740 *in* R.C. Moore (ed.), Treatise on Invertebrate Paleontology, Part N, Mollusca 6, v. 1: The
741 University of Kansas Press, Lawrence, Kansas, and The Geological Society of America, Boulder,
742 Colorado, 490 p.
743 CRIPPA, G., ANGIOLINI, L., BOTTINI, C., ERBA, E., FELLETTI, F., FRIGERIO, C., HENNISSEN, J.A.I.,
744 LENG, M.J., PETRIZZO, M.R., RAFFI, I., RAINERI, G., AND STEPHENSON, M.H., 1916, Seasonality
745 fluctuations recorded in fossil bivalves during the early Pleistocene: Implications for climate
746 change: Palaeogeography. Palaeoclimatology, Palaeoecology, v. 446, p. 234–251, doi:
747 10.1016/j.palaeo.2016.01.029.
748 CUMMINS, R., JR., 1971, Calico scallops of the southeastern United States, 1959–1969: Special
749 Scientific Report—Fisheries No. 6, United States Department of Commerce, Seattle, Washington,
750 22 p.

DE WINTER, N.J., WITBAARD, R., KOCKEN, I.J., MÜLLER, I.A., GUO, J., GOUDSMIT, B., AND ZIEGLER, M., 2022, Temperature dependence of clumped isotopes (Δ_{47}) in aragonite: Geophysical Research Letters, v. 49, number e2022GL099479, doi: 10.1029/2022GL099479.

DOUGLAS, P.M., AFFEK, H.P., IVANY, L.C., AND PAGANI, M., 2014. Pronounced zonal heterogeneity in Eocene southern high-latitude sea surface temperatures: Proceedings of the National Academy of Sciences of the United States of America, v. 11, p. 6582–6587, doi: 10.1073/pnas.1321441111.

DOWSETT, H.J., ROBINSON, M.M., FOLEY, K.M., HERBERT, T.D., OTTO–BLIESNER, B.L., AND SPIVEY, W., 2019, The mid-Piacenzian of the North Atlantic Ocean: Stratigraphy, v. 16, p. 119–144, doi: 10.29041/strat.16.3.119-144.

DOWSETT, H.J., ROBINSON, M.M. FOLEY, K.M., AND HERBERT, T.D., 2021, The Yorktown Formation: Improved stratigraphy, chronology, and paleoclimate interpretations from the U.S. Mid-Atlantic Coastal Plain: Geosciences, v. 11, number 486, doi: 10.3390/geosciences11120486.

DUBAR, J.R., 1974, Summary of the Neogene stratigraphy of southern Florida, *in* R.Q. Oaks and J.R. DuBar (eds.), Post-Miocene Stratigraphy Central and Southern Atlantic Coastal Plain: Utah State University Press, Logan, Utah, p. 206–231.

FEATHERSTONE, A.M., BUTLER, P.G., PEHARDA, M.P., CHAUVAUD, L., AND THÉBAULT, J., 2017, Influence of riverine input on the growth of *Glycymeris glycymeris* in the Bay of Brest, North-West France: PLoS ONE, v. 12, number 0189782 (19 p.), 3.9 MB, doi: 10.1371/journal.pone.0189782.

FEATHERSTONE, A.M., BUTLER, P.G., SCHÖNE, B.R., PEHARDA, M., AND THÉBAULT, J., 2020, A 45-year sub-annual reconstruction of seawater temperature in the Bay of Brest, France, using the shell oxygen isotope composition of the bivalve *Glycymeris glycymeris*: Holocene, v. 30, p. 3-12, doi: 10.1177/0959683619865592.

FÜLLENBACH, C.S., SCHÖNE, B.R., AND MERTZ-KRAUS., R., 2015, Strontium/lithium ratio in shells of *Cerastoderma edule* (Bivalvia) - A new potential temperature proxy for brackish environments: Chemical Geology, v. 417, p. 341–355, doi: 10.1016/j.chemgeo.2015.10.030.

777 GILBERT, P.U., BERGMANN, K.D., MYERS, C.E., MARCUS, M.A., DEVOL, R.T., SUN, C.Y.,
778 BLONSKY, A.Z., TAMRE, E., ZHAO, J., KARAN, E.A., AND TAMURA, N., 2017. Nacre tablet
779 thickness records formation temperature in modern and fossil shells: Earth and Planetary Science
780 Letters, v. 460, p. 281–292, doi: 10.1016/j.epsl.2016.11.012.
781 GILLIKIN, D.P., LORRAIN, A., MENG, L., AND DEHAIRS, F., 2007. A large metabolic carbon
782 contribution to the $\delta^{13}C$ record in marine aragonitic bivalve shells: Geochimica et Cosmochimica
783 Acta, v. 71, p. 2936–2946, doi: 10.1016/j.gca.2007.04.003.
784 GIMENEZ, L.H., DOLDAN, M.S., ZAIDMAN, P.C., AND MORSAN, E.M., 2020, Age and growth
785 of *Glycymeris longior* (Sowerby, 1832) clam at the southern edge of its distribution (Argentine
786 Sea): Helgoland Marine Research, v. 74, number 2 (10 p), 1.46 KB, doi: 10.1186/s10152-020-
787 0534-x. Checked April 2023.
788 GONFIANTINI, R., STICHLER, W., AND ROZANSKI,, K., 1995, Standards and intercomparison materials
789 distributed by the International Atomic Energy Agency for stable isotope measurements, *in*
790 International Atomic Energy Agency, Reference and Intercomparison Materials for Stable Isotopes
791 of Light Elements: IAEA-TECDOC-825, Vienna, Austria, p. 13–29.
792 GOOGLE EARTH PRO 7.3, 2022, 34.23° N, 77.08° W, elevation –27 m,
793 https://www.google.com/earth/versions/~earth-pro. Checked August 2023.
794 GROSSMAN, E.L. AND KU, T., 1986, Oxygen and carbon isotope fractionation in biogenic aragonite:
795 Temperature effects: Chemical Geology (Isotope Geoscience Section), v. 59, p. 59–74, doi:
796 10.1016/0009-2541(86)90044-6.
797 HARWOOD, A.J.P., DENNIS, P.F., MARCA, A.D., PILLING, G.M., AND MILLNER, R.S., 2008, The
798 oxygen isotope composition of water masses within the North Sea: Estuarine Coastal and Shelf
799 Science, v. 78, p. 353–359, doi: 10.1016/j.ecss.2007.12.010.
800 HESTERBERG, S.G., HERBERT, G.S., PLUCKHAHN, T.J., HARKE, R.M., AL-QATTAN, N.M., DUKE, C.T.,
801 MOORE, E.W., SMITH, M.E., DELGADO, A.C., AND SAMPSON, C.P., 2020, Prehistoric baseline
802 reveals substantial decline of oyster reef condition in a Gulf of Mexico conservation priority area:

Biology Letters, v. 16, number 20190865 (5 p.), 556.6 KB, doi: 10.1098/rsbl.2019.0865. Checked April 2023.

HÖCHE, N., PEHARDA, M., WALLISER, E.O., AND SCHÖNE, B.R., 2020, Morphological variations of crossed-lamellar ultrastructures of *Glycymeris bimaculata* (Bivalvia) serve as a marine temperature proxy: Estuarine Coastal and Shelf Science, v. 237, number 106658, doi: 10.1016/j.ecss.2020.106658.

HÖCHE, N., WALLISER, E.O., DE WINTER, N.J., WITBAARD, R., AND SCHÖNE, B.R., 2021, Temperature-induced microstructural changes in shells of laboratory-grown *Arctica islandica* (Bivalvia): Plos One, v. 16, e0247968, doi: 10.1371/journal.pone.0247968.

HUYGHE, D., DAËRON, M., DE RAFELIS, M., BLAMART, D., SÉBILO, M., PAULET Y.-M., AND LARTAUD F., 2021, Clumped isotopes in modern marine bivalves: Geochimica et Cosmochimica Acta, v. 316, p. 41–58, doi: 10.1016/j.gca.2021.09.019.

IVANY, L.C., PATTERSON, W.P., AND LOHMANN, K.C., 2000, Cooler winters as a possible cause of mass extinctions at the Eocene/Oligocene boundary: Nature, v. 407, p. 887-890, doi: 10.1038/35038044.

ISHII, M., SHOUJI, A., SUGIMOTO, S., AND MATSUMOTO, T., 2005, Objective analyses of sea-surface temperature and marine meteorological variables for the 20th century using ICOADS and the Kobe collection: International Journal of Climatology, v. 25, p. 865–879, doi: 10.1002/joc.1169.

JOHNSON, A.L.A., VALENTINE, A., LENG, M.J., SLOANE, H.J., SCHÖNE, B.R., AND BALSON, P.S., 2017, Isotopic temperatures from the early and mid-Pliocene of the US Middle Atlantic Coastal Plain, and their implications for the cause of regional marine climate change: PALAIOS, v. 32, p. 250–269, doi: 10.2110/palo.2016.080.

JOHNSON, A.L.A., VALENTINE, A.M., LENG, M.J., SCHÖNE, B.R., SLOANE, H.J., 2019, Life history, environment and extinction of the scallop *Carolinapecten eboreus* (Conrad) in the Plio-Pleistocene of the U.S. eastern seaboard: PALAIOS, v. 34, p. 49–70, doi: 10.2110/palo.2018.056.

828 JOHNSON, A.L.A., HARPER, E.M., CLARKE, A., FEATHERSTONE, A.C., HEYWOOD, D.J., RICHARDSON,
829 K.E, SPINK, J.O. AND THORNTON, L.A.H., 2021, Growth rate, extinction and survival amongst late
830 Cenozoic bivalves of the North Atlantic: Historical Biology, v. 33, p. 802-813, doi:
831 10.1080/08912963.2019.1663839.
832 JOHNSON, A.L.A., VALENTINE, A.M., SCHÖNE, B.R., LENG, M.J., AND GOOLAERTS S, 2022,
833 Sclerochronological evidence of pronounced seasonality from the Pliocene of the southern North
834 Sea Basin and its implications: Climate of the Past, v. 18, p. 1203-1229, doi:10.5194/cp-18-1203-
835 2022.
836 KILLAM, D., AL-NAJJAR, T., AND CLAPHAM, M., 2021, Giant clam growth in the Gulf of Aqaba is
837 accelerated compared to fossil populations. Proceedings of the Royal Society of London, Series B,
838 v. 288, number 20210991 (8 p.), 695.9 KB, doi: 10.1098/rspb.2021.0991. Checked April 2023.
839 KIRBY M.X. AND MILLER, H.M., 2005, Response of a benthic suspension feeder (*Crassostrea*
840 *virginica* Gmelin) to three centuries of anthropogenic eutrophication in Chesapeake Bay:
841 Estuarine, Coastal and Shelf Science, v. 62, p. 679–689, doi: 10.1016/j.ecss.2004.10.004.
842 KITTLE, B.A., PORTELL, R.W., LEE, H.G., AND ROBERTS, S.W., 2013, Mollusca – Nashua Formation
843 (Late Pliocene to Early Pleistocene): Florida Fossil Invertebrates, Part 15, Florida Paleontological
844 Society, University of Florida, Gainesville, Florida, 40 p.
845 KRANTZ, D.E., WILLIAMS, D.F., AND JONES, D.S., 1987, Ecological and paleoenvironmental
846 information using stable isotope profiles from living and fossil molluscs: Palaeogeography,
847 Palaeoclimatology, Palaeoecology, v. 58, p. 249–266, doi: 10.1016/0031-0182(87)90064-2.
848 KRANTZ, D.E., KRONICK, A.T., AND WILLIAMS, D.F., 1988, A model for interpreting continental-
849 shelf hydrographic process from the stable isotope and cadmium:calcium profiles of scallop shells:
850 Palaeogeography, Palaeoclimatology, Palaeoecology, v. 64, p. 123–140, doi: 10.1016/0031-
851 0182(88)90002-8.

852 LEE, T.N., YODER, J.A., AND ATKINSON, L.P., 1991, Gulf Stream frontal eddy influence on
853 productivity of the southeast U.S. continental shelf: Journal of Geophysical Research: Oceans, v.
854 96, p. 22191–22205, doi: 10.1029/91jc02450.
855 LEGRANDE, A.N. AND SCHMIDT, G.A., 2006, Global gridded data set of the oxygen isotopic
856 composition in seawater: Geophysical Research Letters, v. 33, L12604 (5 p.), 808.9 KB, doi:
857 10.1029/2006GL026011.
858 LOCARNINI, R.A.., MISHONOV, A.V., BARANOVA, O.K., BOYER, T.P., ZWENG, M.M., GARCIA, H.E.,
859 REAGAN, J.R., SEIDOV, D., WEATHERS, K.W., PAVER, C.R, AND SMOLYAR, I.V., 2018, World
860 Ocean Atlas 2018, Volume 1: Temperature (A. Mishonov, Technical Editor): NOAA Atlas
861 NESDIS 81, 52 p., https://www.ncei.noaa.gov/sites/default/files/2022-06/woa18_vol1.pdf.
862 Checked July 2023.
863 LOCKWOOD, R. AND MANN, R., 2019, A conservation palaeobiological perspective on Chesapeake
864 Bay oysters: Philosophical Transactions of the Royal Society of London, Series B, v. 374 number
865 20190209 (11 p.), 627.1 KB, doi: 10.1098/rstb.2019.0209.
866 MARCHAIS, V., RICHARD, J., JOLIVET, A., FLYE-SAINTE-MARIE, J., THÉBAULT, J., JEAN, F., RICHARD,
867 P., PAULET, Y.-M., CLAVIER, J., AND CHAUVAUD, L., 2015, Coupling experimental and field-based
868 approaches to decipher carbon sources in the shell of the great scallop, *Pecten maximus* (L.):
869 Geochimica et Cosmochimca Acta, v. 168, p. 58–69, doi: 10.1016/j.gca.2015.07.010.
870 MILANO, S., SCHÖNE, B.R., AND WITBAARD, R., 2017a, Changes of shell microstructural
871 characteristics of *Cerastoderma edule* (Bivalvia)—A novel proxy for water temperature:
872 Palaeogeography, Palaeoclimatology, Palaeoecology, v. 465, p. 395–406, doi:
873 10.1016/j.palaeo.2015.09.051.
874 MILANO, S., NEHRKE, G., WANAMAKER, A.D., BALLESTA-ARTERO, I., BREY, T., AND SCHÖNE, B.R.,
875 2017b, The effects of environment on *Arctica islandica* shell formation and architecture:
876 Biogeosciences, v. 14, p. 1577–1591, doi: 10.5194/bg-14-1577-2017.

877 MOSS, D.K., IVANY, L.C., JUDD, E.J., CUMMINGS, P.C., BEARDEN, C.E., KIM, W.-J., ARTRUC, E.G.,
878 AND DRISCOLL, J.R., 2016, Lifespan, growth rate, and body size across latitude in marine Bivalvia,
879 with implications for Phanerozoic evolution: Proceedings of the Royal Society of London, Series
880 B, v. 283, number 20161364 (7 p.), 771.7 KB, doi:10.1098/rspb.2016.1364. Checked April 2023.
881 MOSS, D.K., IVANY, L.C., AND JONES, D.S., 2021. Fossil bivalves and the sclerochronological
882 reawakening: Paleobiology, v. 47, p. 551–573, doi: 10.1017/pab.2021.16.
883 NEMETH, A. AND KERN, Z., 2018, Sclerochronological study of a *Glycymeris vangentsumi* population
884 from the Madeira Islands: Frontiers in Earth Science, v. 6, number 76 (13 p.), 3.0 MB, doi:
885 10.3389/feart.2018.00076. Checked April 2023.
886 NICOL, D., 1953, A study of the polymorphic species *Glycymeris americana*: Journal of
887 Paleontology, v. 27, p. 451–455.
888 OBIS (OCEAN BIODIVERSITY INFORMATION SYSTEM), undated, *Glycymeris* da Costa, 1778,
889 https://obis.org/taxon/138035. Checked April 2023.
890 PALMER, K.L., MOSS, D.K., SURGE, D., AND TUREK, S., 2021, Life history patterns of modern and
891 fossil *Mercenaria* spp. from warm vs. cold climates: Palaeogeography, Palaeoclimatology,
892 Palaeoecology, v. 566, number 110227 (13 p.), 2.5 MB, doi: 10.1016/j.palaeo.2021.110227.
893 PEHARDA, M., CRNCEVIĆ, M., BUSELIĆ, I., RICHARDSON, C.A., AND EZGETA-BALIĆ, D., 2012, Growth
894 and longevity of *Glycymeris nummaria* (Linnaeus, 1758) from the eastern Adriatic, Croatia:
895 Journal of Shellfish Research, v. 31, p. 947–950, doi: 10.2983/035:031.0406.
896 PEHARDA, M., BLACK, B.A., PURROY, A., AND MIHANOVIĆ, H., 2016, The bivalve *Glycymeris pilosa*
897 as a multidecadal environmental archive for the Adriatic and Mediterranean Seas: Marine
898 Environmental Research, v. 119, p. 79–87, doi: 10.1016/j.marenvres.2016.05.022.
899 PEHARDA, M., THÉBAULT, J., MARKULIN, K., SCHÖNE, B.R., JANEKOVIĆ, I., AND CHAUVAUD, L.,
900 2019a, Contrasting shell growth strategies in two Mediterranean bivalves revealed by oxygen-
901 isotope ratio geochemistry: The case of *Pecten jacobaeus* and *Glycymeris pilosa*: Chemical
902 Geology, v. 526, p. 23–35, doi:10.1016/j.chemgeo.2017.09.029.

PEHARDA, M., WALLISER, E.O., MARKULIN, K., PURROY, A., UVANOVIĆ, H., JANEKOVIĆ, I., ŽUPAN, I., VILIBIĆ, I., AND SCHÖNE, B.R., 2019b, *Glycymeris pilosa* (Bivalvia) – A high-potential geochemical archive of the environmental variability in the Adriatic Sea: Marine Environmental Research, v. 150, number 104759 (14 p.), 3.7 MB, doi: 10.1016/j.marenvres.2019.104759.

PIETRAFESA, L.J., MORRISON, J.M., MCCANN, M.P., CHURCHILL, J., BÖHM, E., and HOUGHTON, R.W., 1994, Water mass linkages between the Middle and South Atlantic Bights: Deep Sea Research, Part II-Topical Studies in Oceanography, v. 41, p. 365–389, doi: 10.1016/0967-0645(94)90028-0.

PORTER, H.J. AND WOLFE, D.A., 1971, Mollusca from the North Carolina commercial fishing grounds for the calico scallop *Argopecten gibbus* (Linné): Journal de Conchyliologie, v. 109, p. 91–109.

RAMSAY, K., KAISER, M.J., RICHARDSON, C.A., VEALE, L.O., AND BRAND, A.R., 2000, Can shell scars on dog cockles (*Glycymeris glycymeris* L.) be used as an indicator of fishing disturbance?: Journal of Sea Research, v. 43, p. 167–176, doi: 10.1016/S1385-1101(00)00006-X.

REYNOLDS, D.J., BUTLER, P.G., WILLIAMS, S.M., SCOURSE, J.D., RICHARDSON, C.A., WANAMAKER, A.D. JR., AUSTIN, W.E.N., CAGE, A.G., AND SAYER, M.D.J., 2013, A multiproxy reconstruction of Hebridean (NW Scotland) spring sea surface temperatures between AD 1805 and 2010: Palaeogeography, Palaeoclimatology, Palaeoecology, v. 386, p. 275–285, doi: 10.1016/j.palaeo.2013.05.029.

REYNOLDS, D.J., HALL, I.R., SLATER, S.M., SCOURSE, J.D., HALLORAN, P.R., AND SAYER, M.D.J., 2017a, Reconstructing past seasonal to multicentennial-scale variability in the NE Atlantic ocean using the long-lived marine bivalve mollusk *Glycymeris glycymeris*: Paleoceanography, v. 32, p. 1153–1173, doi: 10.1002/2017PA003154.

REYNOLDS, D.J., RICHARDSON, C.A., SCOURSE, J.D., BUTLER, P.G., HOLLYMAN, P., ROMÁN-GONZÁLEZ, A., AND HALL, I.R., 2017b, Reconstructing North Atlantic marine climate variability

928 using an absolutely-dated sclerochronological network: Palaeogeography, Palaeoclimatology,
929 Palaeoecology, v. 465, p. 333–346, doi:10.1016/j.palaeo.2016.08.006.
930 RICHARDSON, C.A. AND WALKER, P., 1993, The age structure of a population of the hard-shell clam,
931 *Mercenasria mercenaria* from Southampton Water, England, derived from acetate peel replicas of
932 shell sections: ICES Journal of Marine Science, v. 48, p. 229–236, doi: 10.1093/icesjms/48.2.229.
933 RIGGS, S.R., 1984, Paleoceanographic model of Neogene phosphorite deposition, U.S. Atlantic
934 continental margin: Science, v. 223, p. 123–131, doi: 10.1126/science.223.4632.123.
935 ROYER, C., THÉBAULT, J., CHAUVAUD, L., OLIVIER, F., 2013, Structural analysis and
936 paleoenvironmental potential of dog cockle shells (*Glycymeris glycymeris*) in Brittany, northwest
937 France: Palaeogeography, Palaeoclimatology, Palaeoecology, v. 373, p. 123–132,
938 doi:10.1016/j.palaeo.2012.01.033.
939 SCHÖNE, B.R., 2013, *Arctica islandica* (Bivalvia): A unique paleoenvironmental archive of the
940 northern North Atlantic Ocean: Global and Planetary Change, v. 111, p. 199–225, doi:
941 10.1016/j.gloplacha.2013.09.013.
942 SCHÖNE, B.R., FLESSA, K.W., DETTMAN, D.L., AND GOODWIN, D.H., 2003, Upstream dams and
943 downstream clams: growth rates of bivalve mollusks unveil impact of river management on
944 estuarine ecosystems (Colorado River Delta, Mexico): Estuarine, Coastal and Shelf Science, v. 58,
945 p. 715–726, doi: 10.1016/S0272-7714(03)00175-6.
946 SCHÖNE, B.R., DUNCA, E., FIEBIG, J., PFEIFFER, M., 2005, Mutvei's solution: An ideal agent for
947 resolving microgrowth structures of biogenic carbonates: Palaeogeography, Palaeoclimatology,
948 Palaeoecology, v. 228, p. 149–166, doi: 10.1016/j.palaeo.2005.03.054.
949 SIME, J.A. AND KELLEY, P.H., 2016, Common mollusk genera indicate interactions with their
950 predators were ecologically stable across the Plio-Pleistocene extinction: Palaeogeography,
951 Palaeoclimatology, Palaeoecology, v. 463, p. 216–229, doi: 10.1016/j.palaeo.2016.10.012.
952 THOMAS, R.D.K., 1975, Functional morphology, ecology and evolutionary conservatism in the
953 Glycymerididae (Bivalvia): Palaeontology, v. 18, p. 217–254.

954 THOMAS, R.D.K., 1976, Gastropod predation on sympatric Neogene species of *Glycymeris* (Bivalvia)
955 from the eastern United States: Journal of Paleontology, v. 50, p. 488–499.
956 VALENTINE, A., JOHNSON, A.L.A., LENG, M.J., SLOANE, H.J., AND BALSON, P. S., 2011, Isotopic
957 evidence of cool winter conditions in the mid-Piacenzian (Pliocene) of the southern North Sea
958 Basin, Palaeogeography, Palaeoclimatology, Palaeoecology, v. 309, p. 9–16, doi:
959 10.1016/j.palaeo.2011.05.015.
960 VERMEIJ, G.J., 1987, Evolution and Escalation: An Ecological History of Life: Princeton University
961 Press, Princeton, New Jersey, 527 p.
962 WALLISER, E.O., SCHÖNE, B.R., TÜTKEN, T., ZIRKEL, J., GRIMM, K.I., AND PROSS, J., 2015, The
963 bivalve *Glycymeris planicostalis* as a high-resolution paleoclimate archive for the Rupelian (Early
964 Oligocene) of central Europe: Climate of the Past, v. 11, p. 653–668, doi: 10.5194/cp-11-653-
965 2015.
966 WALLISER, E.O., LOHMANN, G., NIEZGODZKI, I., TÜTKEN, T., AND SCHÖNE, B.R., 2016, Response of
967 Central European SST to atmospheric pCO_2 forcing during the Oligocene - A combined proxy
968 data and numerical climate model approach: Palaeogeography, Palaeoclimatology, Palaeoecology,
969 v. 459, p. 552–569, doi: 10.1016/j.palaeo.2016.07.033.
970 WARD, L.W. AND BLACKWELDER, B.W., 1987, Late Pliocene and early Pleistocene Mollusca from
971 the James City and Chowan River formations at the Lee Creek Mine, *in* C.E. Ray (ed.), Geology
972 and Paleontology of the Lee Creek Mine, North Carolina, II: Smithsonian Contributions to
973 Paleobiology, n. 61, p. 113–283.
974 WARD, L.W., BAILEY, R.H., AND CARTER, J.G., 1991, Pliocene and early Pleistocene stratigraphy,
975 depositional history, and molluscan paleobiogeography of the Coastal Plain, *in* J.W. Horton, Jr.
976 and V.A. Zullo (eds.), The geology of the Carolinas: University of Tennessee Press, Knoxville,
977 Tennessee, p. 274–289.
978 WICHERN, N.M.A., DE WINTER, N.J., JOHNSON, A.L.A., GOOLAERTS, S., WESSELINGH, F., HAMERS,
979 M.F., KASKES, P., CLAEYS, P., AND ZIEGLER, M., 2023, The fossil bivalve *Angulus benedeni*

benedeni: a potential seasonally resolved stable isotope-based climate archive to investigate Pliocene temperatures in the southern North Sea basin: Biogeosciences, v. 20, p. 2317–2345, doi: 10.5194/bg-20-2317-2023.

WILLIAMS, M., HAYWOOD, A.M., HARPER, E.M., JOHNSON, A.L.A., KNOWLES, T., LENG, M.J., LUNT, D.J., OKAMURA, B., TAYLOR, P.D. AND ZALAZIEWICZ, J.:, 2009, Pliocene climate and seasonality in North Atlantic shelf seas, Philosophical Transactions of the Royal Society of London, Series A, v. 367, p. 85–108, doi: 10.1098/rsta.2008.0224.

WoRMS (WORLD REGISTER OF MARINE SPECIES), undated, *Glycymeris americana* (DeFrance, 1826), https://www. marinespecies.org/aphia.php?p=taxdetails&id=420727. Checked July 2023.

YAMAOKA, Y., KONDO, Y., AND ITO, H., 2016, Rate and pattern of shell growth of *Glycymeris fulgurata* and *Glycymeris vestita* (Bivalvia: Glycymerididae) in Tosa Bay as inferred from oxygen isotope analysis: Venus, v. 74, p. 61–69, doi: 10.18941/venus.74.3-4_61.

ZENG, X. AND HE, R., 2016. Gulf Stream variability and a triggering mechanism of its large meander in the South Atlantic Bight: Journal of Geophysical Research: Oceans, v. 121, p. 8021–8038, doi: 10.1002/2016JC012077.

ZHANG, J.Z. AND PETERSEN, S.V., 2023, Clumped and oxygen isotope sclerochronology methods tested in the bivalve *Lucina pensylvanica*: Chemical Geology, v. 620, number 121346, doi: 10.1016/j.chemgeo.2023.121346. Checked April 2023.

ZWENG, M.M., REAGAN, J.R., SEIDOV, D., BOYER, T.P., LOCARNINI, R.A., GARCIA, H.E., MISHONOV, A.V., BARANOVA, O.K., WEATHERS, K.W., PAVER, C.R. AND SMOLYAR, I.V., 2019, World Ocean Atlas 2018, Volume 2: Salinity (A. Mishonov, Technical Editor): NOAA Atlas NESDIS 82, 50 p., https://www.ncei.noaa.gov/sites/default/files/2022-06/woa18_vol2.pdf. Checked July 2023.

FIGURE CAPTIONS

1005 FIG. 1.—The studied specimens of G*lycymeris americana*, showing the locations of sample holes in
1006 FL1 and of sample grooves (numbered) in NA1, together with the positions of prominent growth
1007 lines (filled green triangles) and of light (white bars) and dark (black bars) shell material in the latter;
1008 from the heights spanned by the first and last of the light/dark pairs depicted it is probable that one
1009 more pair is represented in early ontogeny and two more in late ontogeny. Specimens are shown as
1010 greyscale images with dorsal at the top (height is the dorso-ventral dimension and length the
1011 perpendicular dimension in the plane of the illustration). Boundary between outer (to right) and inner
1012 shell layers shown by yellow dashed line in inset for FL1; outer layer also identified in Figure 7.
1013 Scale applies to main images, not insets.
1014
1015 FIG. 2.—Collection locations of studied modern (squares) and early Pleistocene (circles) specimens
1016 of *Glycymeris americana* from the eastern U.S. (details in Tables 1 and 2, respectively), with
1017 abbreviated names for states. Those referred to herein are VA (Virginia), NC (North Carolina), SC
1018 (South Carolina), GA (Georgia) and FL (Florida).
1019
1020 FIG. 3.—HDR images (with enhanced contrast) of whole-shell and hinge-plate cross-sections of the
1021 modern shells NC1 (from North Carolina) and FL2 (from Florida). The whole-shell images are of
1022 surfaces treated with Mutvei's solution; the hinge-plate images are of (from left) acetate peels of
1023 unstained surfaces, acetate peels of surfaces stained with Alizarin Red, surfaces treated with
1024 Mutvei's solution and untreated surfaces (seen in greyscale). Hinge banding is scarcely visible in the
1025 peels from NC1 but is clear in the dorsal part of the same from FL2 and in the dorsal part of the
1026 Mutvei-treated and untreated surfaces of both specimens. The sharply-defined bands in the peels
1027 from FL2 approximately correspond to more gradationally-bounded light/dark pairs of bands in the
1028 Mutvei-treated and untreated surfaces. The lines between numbered peel-bands (taken to be annual
1029 increments; see text) occupy a position within the dark bands seen in Mutvei-treated and untreated
1030 surfaces, hence the numbered 'pairs' in these surfaces (also in NC1) have been delimited midway

through each dark band and are actually constituted by a whole light band and two halves of dark bands. Note that the Mutvei-treated whole-shell cross-section of NC1 shows 4 zones of darker-blue colouration (db) which may be equivalent to the 4 dark bands in the similarly treated hinge-plate cross-section. White spots in peel images are bubbles.

FIG. 4.—HDR images (with enhanced contrast) of whole-shell and hinge-plate cross-sections of the modern shells NC2 (from North Carolina) and FL1 (from Florida). The whole-shell images are of surfaces treated with Mutvei's solution; the hinge-plate images are of (left) surfaces treated with Mutvei's solution and (right) untreated surfaces (seen in greyscale). Annual increments identified and delimited as in Figure 3 (see text for further details). Although darker-blue zones can be discerned in the Mutvei-treated whole-shell cross-sections, as in NC1 (Fig. 3), the number (< 4 in NC2, < 7 in FL1) is in both cases lower than the number of dark bands (9 in NC2, 10 in FL1) in the hinge plate.

FIG. 5.—HDR images (greyscale; with enhanced contrast) of untreated hinge-plate cross-sections of the early Pleistocene shells JC3, JC4 (both from North Carolina) and BC1 (from Florida). Annual increments identified and delimited as in Figure 3; not indicated individually above age 20.

FIG. 6.—HDR image (greyscale; with enhanced contrast) of untreated whole-shell cross-section of the modern North Carolina shell NC1. Note the fine-scale banding, reflecting a sub-annual periodicity, in this 31-mm-high, 5-year-old individual (see Fig. 9). Sample holes also evident.

FIG. 7.—HDR image of acetate peel from Alizarin Red-stained whole-shell cross-section of JC4 (early Pleistocene, North Carolina), with insets (not to same scale) showing details in the hinge plate (lower right as seen) and in the outer layer (OL) of the main part of the shell. Note the very clear increments (presumed to be annual) in the hinge plate and near the ventral margin (left as seen) in the

1057 main shell, the broader but less clear increments (again presumed to be annual) at a somewhat more
1058 dorsal location (lower height) in the main shell, and the absence of annual increments and presence
1059 of fine increments representing a shorter periodicity at a still more dorsal location (see text for
1060 explanation). White spots and patches are bubbles.
1061
1062 FIG. 8.—Plots of size measurements against age measurements for modern (continuous lines) and
1063 early Pleistocene (dotted lines) specimens of *Glycymeris americana* from Florida (rose) and North
1064 Carolina (mid-blue). Smaller dots represent data from Johnson et al. (2021). **A**) hinge size against
1065 age from hinge increments. **B**) shell height against age from oxygen isotope cycles (years defined by
1066 summer minima).
1067
1068 FIG. 9.—$\delta^{13}C$ (black line) and $\delta^{18}O$ (brick-red line) profiles from the modern (pale blue background)
1069 and early Pleistocene (pale yellow background) shells, together with numbered years (summers) of
1070 growth from $\delta^{18}O$ evidence and the height intervals (grey bars) of dark shell material on the exterior
1071 of the externally sampled specimen NA1. In accordance with common practice, the isotopic axis has
1072 been reversed such that lower $\delta^{18}O$ values (corresponding to higher temperatures) plot towards the
1073 top. Stars indicate positions of large single-point $\delta^{18}O$ excursions, which more probably reflect
1074 contamination by material from other sample sites (i.e. failure to remove every vestige of powder
1075 after drilling) than seasonal extremes of additional annual cycles. [1] = presumed first year.
1076
1077 FIG. 10.—Left-hand plots: mean monthly surface temperature (thin red line) and seafloor
1078 temperature and salinity (thicker red and green line, respectively) for the locations of the modern
1079 shells from direct measurement (as described in 'Methods'). Right-hand plots: temperature profiles
1080 from the modern shells, calculated from the shell $\delta^{18}O$ data in Figure 9 using the relevant annual
1081 mean seafloor value for water $\delta^{18}O$ (see 'Methods') and the equations of Grossman and Ku (1986;
1082 mauve line) and Royer et al. (2013; pink line). Vertical green dotted lines mark the projected

positions of moderate–major external growth breaks in the isotope-sample path. Horizontal red and blue dashed lines mark the respective maximum and minimum directly-measured seafloor temperatures for the location, as recorded in the corresponding left-hand plot.

FIG. 11.—Temperature profiles from the early Pleistocene shells calculated from the shell $\delta^{18}O$ data in Figure 9 using the equation of Grossman and Ku (1986) and water $\delta^{18}O$ values of +0.70‰ (light blue line) and +1.10‰ (orange line). Vertical green dotted lines mark the positions of moderate–major growth breaks. Horizontal red and blue dashed lines mark the modern maximum and minimum seafloor temperatures in North Carolina and Florida (averages of the two values for each state in Fig. 10).

FIG. 12.—Summary statistics for summer (red) and winter (blue) temperatures calculated from minima and maxima, respectively, of $\delta^{18}O$ profiles from all the analysed *Glycymeris americana* specimens apart from JC4 (see text), using the equation of Grossman and Ku (1986). Symbols show the mean seasonal temperature (circles, early Pleistocene; squares, modern), one standard deviation either side of the mean (thick bars), and the range of values, with the sample size indicated alongside. For each of the modern specimens the respective $\delta^{18}O_w$ value for the location (see text) was used in calculation. The water $\delta^{18}O$ ($\delta^{18}O_{w)}$ values of +0.7‰ and +1.1‰ used for the early Pleistocene specimens are the minimum and maximum inferred herein (see text).

TABLE CAPTIONS

TABLE 1.—*Repository, provenance, condition and size information for modern specimens of* Glycymeris americana*. Key to superscripts: a = U.S. National Museum of Natural History; b = Florida Museum of Natural History, University of Florida; c = assumed to have been collected during scallop dredging (see 'Differences in Age Structure of Populations') and hence assigned to the most productive location and depth off Cape Canaveral (Blake and Moyer 1991); d =*

erroneously labelled as from 87 fathoms (159 m) rather than 87 feet (27 m), the depth at the collection location according to Google Earth Pro 7.3 (2022); e = provided as two 10-mm-thick resin-mounted slabs, each showing a section along the dorso-ventral axis (anterior and posterior portions of shell not available); f = length estimated from height.

TABLE 2.—*Repository, provenance, age, condition and size information for fossil specimens of* Glycymeris americana*. Key to superscripts: a = code designated by Johnson et al. (2021) and retained here for cross-referencing purposes; b = University of Derby, Geological Collections; c = Florida Museum of Natural History, University of Florida; d = UD 53384–53389 (JC1–6 of Johnson et al. 2021) and four further valves, including an articulated pair (all UD 53426); e = 1.80–0.77 Ma—see Johnson et al. (2019, online supplemental data file 1) for more precise information on age; f = 2.58–1.80 Ma—the Nashua Formation spans the Pliocene/Pleistocene boundary (Kittle et al. 2013) but only the upper part, equivalent to the Caloosahatchee Formation, yields aragonitic fossils (R.W. Portell, personal communication 2019), hence* G. americana *specimen NA1 is here considered to be Gelasian in age; g = 2.58–0.77 Ma—see Johnson et al. (2019, online supplemental data file 1) for more precise information on age; h = other valve possibly constituted by JC2, which is almost identical in size and provides a very similar increment-based figure for age—see Johnson et al. (2021, online supplemental material).*

TABLE 3.—*Estimated ages (complete years) from hinge-bands or (NA1) from bands on the exterior of the main shell, and from $\delta^{18}O$ cycles. Partial visibility of bands or partial isotopic sampling is indicated by figures in italics, the first being the number of years indicated by bands/$\delta^{18}O$ cycles and the second (in parentheses) the minimum total number projected from the height interval spanned by the last band/isotope cycle (see text for explanation).*

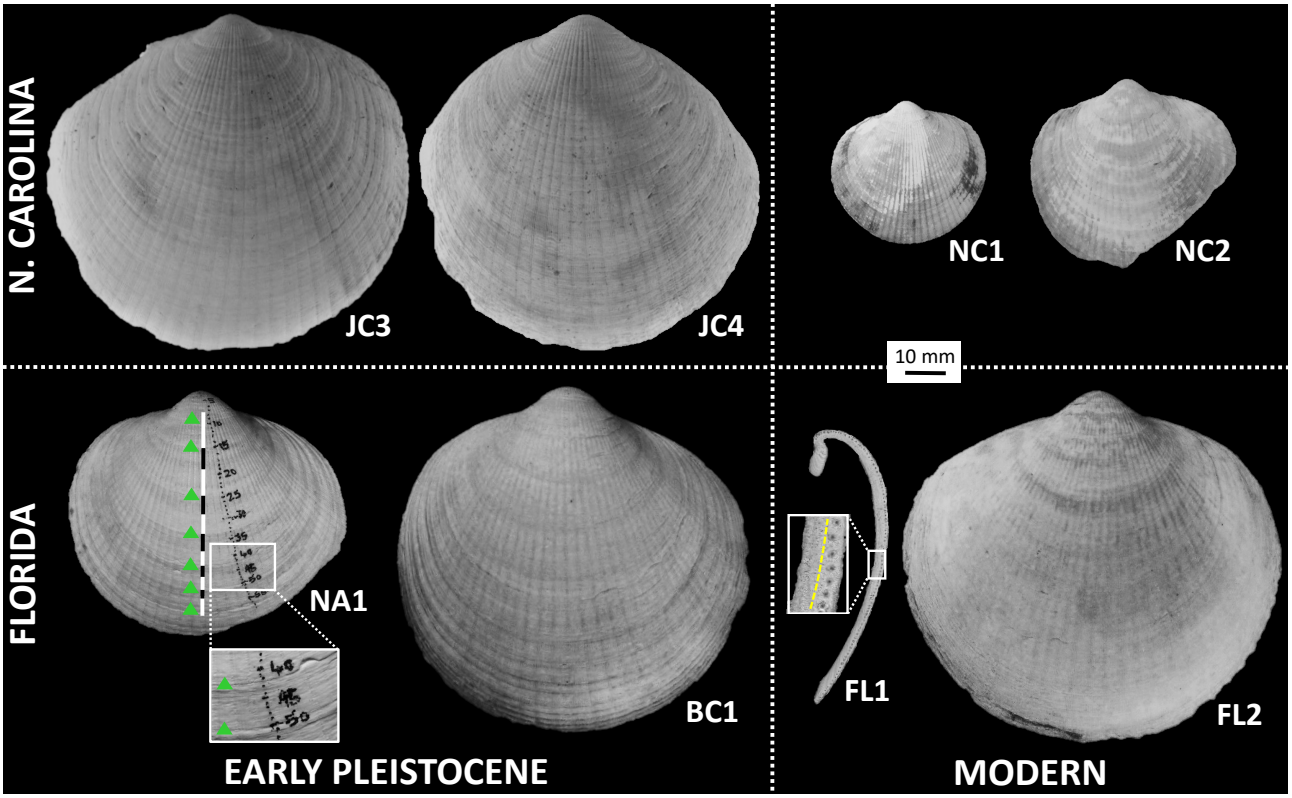
N. CAROLINA
JC3
JC4
NC1
NC2
10 mm
FLORIDA
NA1
BC1
FL1
FL2
EARLY PLEISTOCENE
MODERN

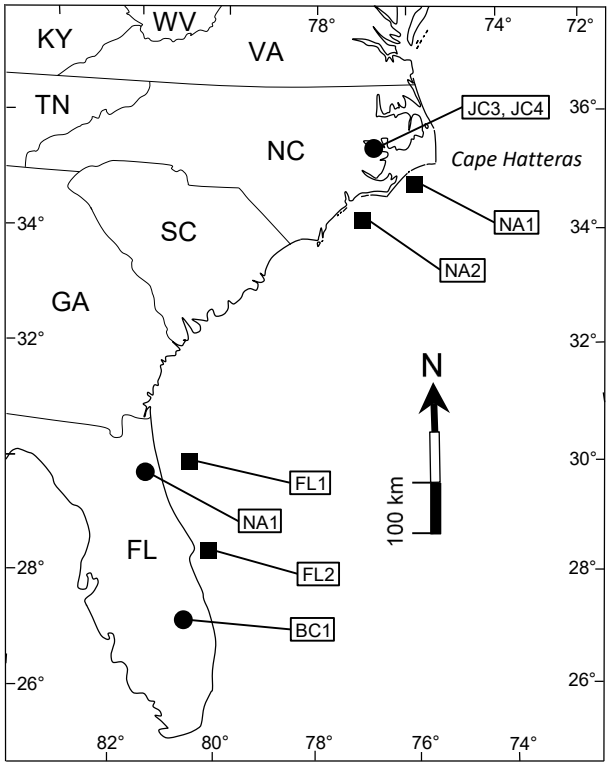
KY
WV
VA
TN
NC
SC
GA
FL
78°
74°
72°
36°
34°
32°
30°
28°
26°
82°
80°
78°
76°
74°
JC3, JC4
Cape Hatteras
NA1
NA2
FL1
NA1
FL2
BC1
N
100 km

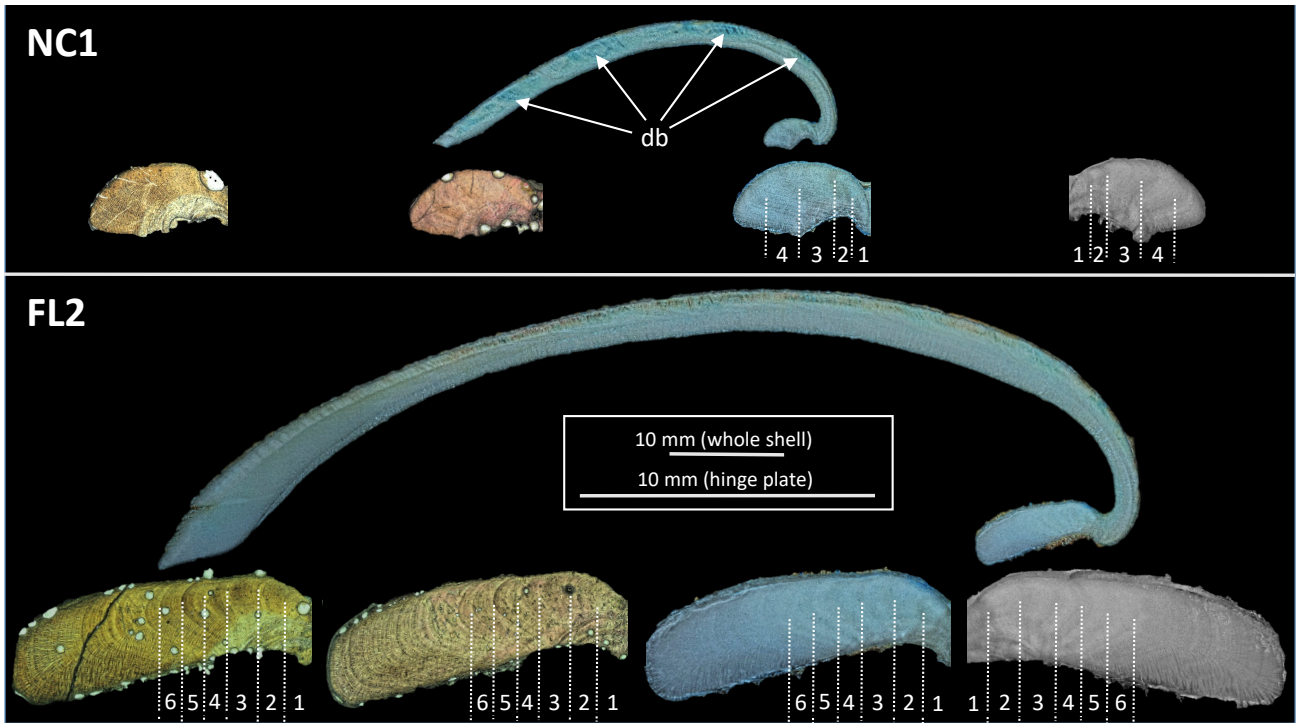
NC1
db
4 3 2 1
1 2 3 4
FL2
10 mm (whole shell)
10 mm (hinge plate)
6 5 4 3 2 1
6 5 4 3 2 1
6 5 4 3 2 1
1 2 3 4 5 6

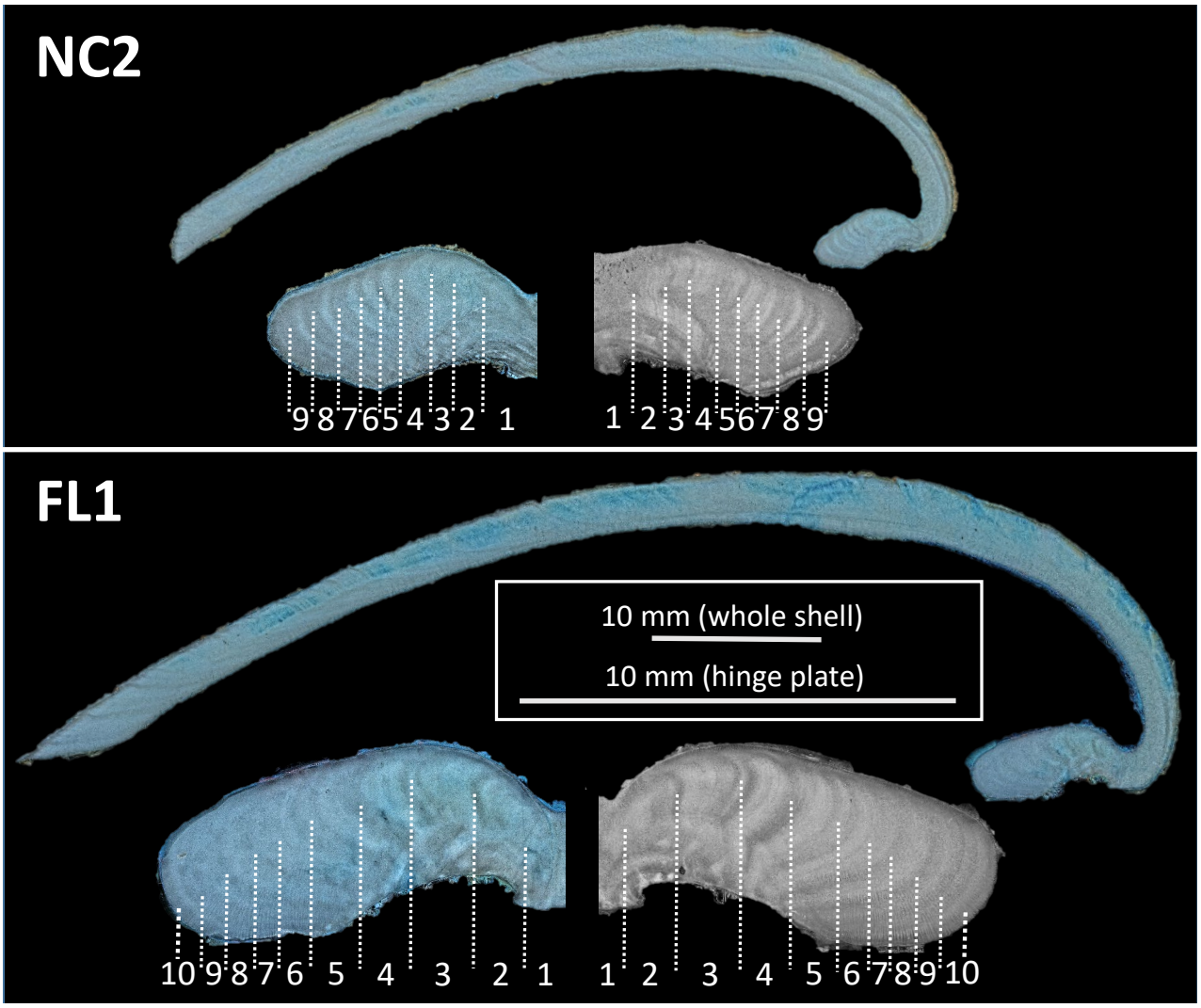
NC2
9 8 7 6 5 4 3 2 1
1 2 3 4 5 6 7 8 9
FL1
10 mm (whole shell)
10 mm (hinge plate)
10 9 8 7 6 5 4 3 2 1
1 2 3 4 5 6 7 8 9 10

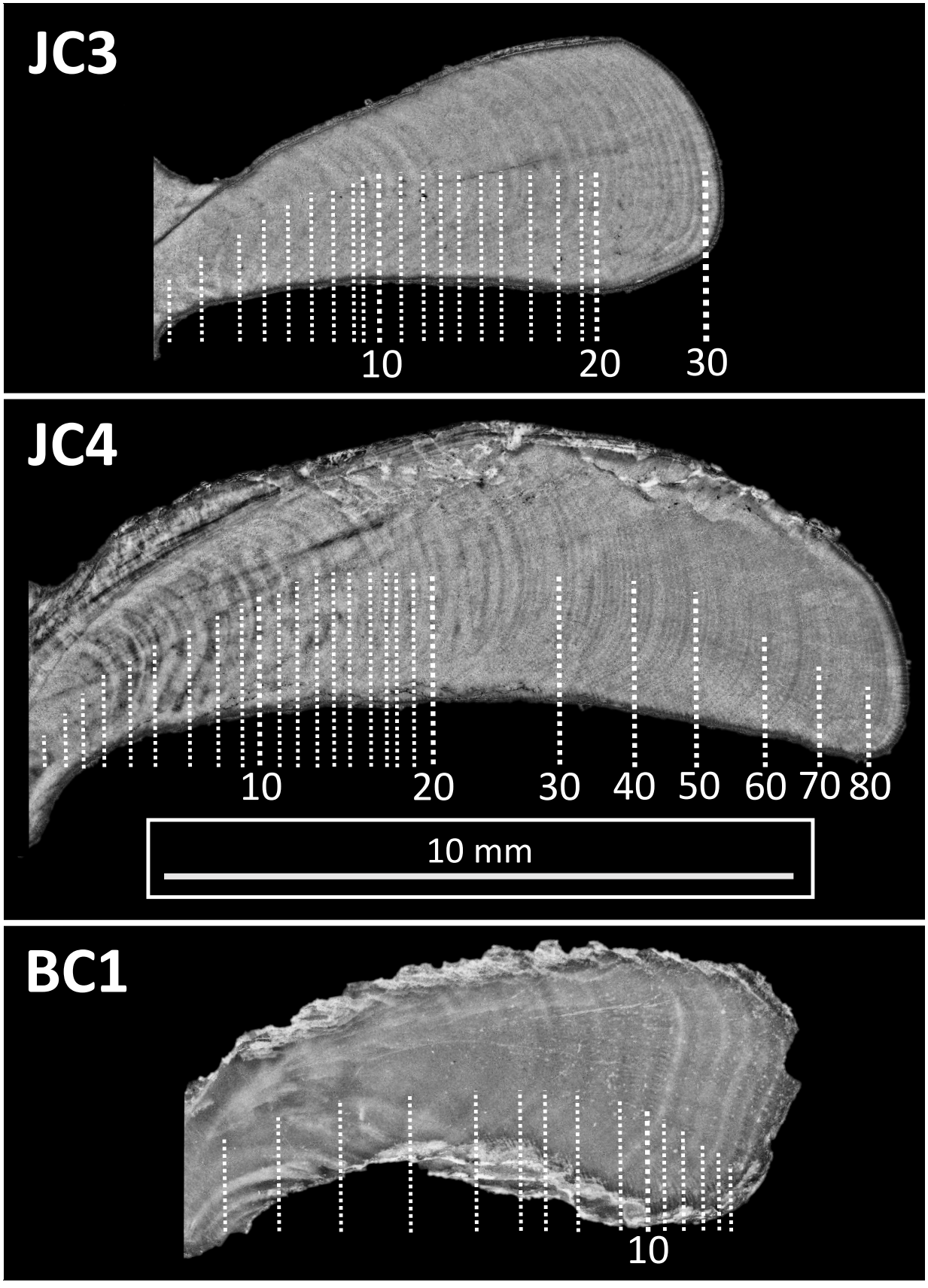
JC3
10
20
30
JC4
10
20
30
40
50
60
70
80
10 mm
BC1
10

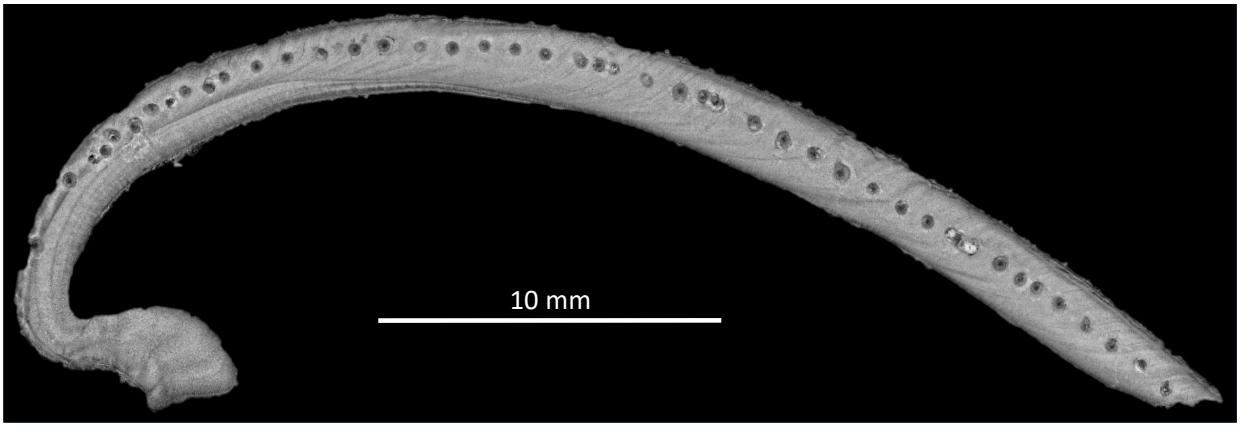
10 mm

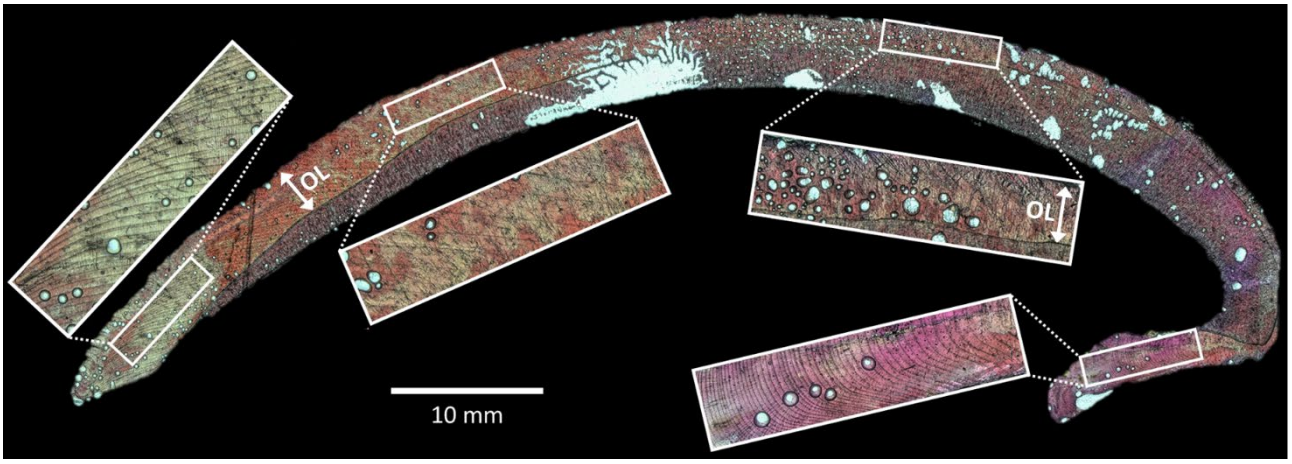
OL
OL
10 mm

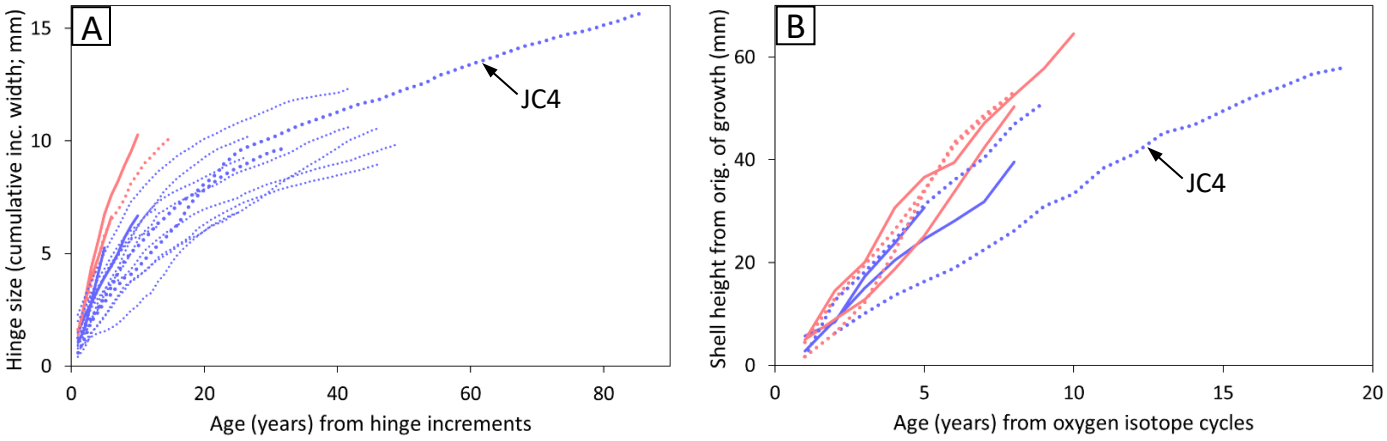
A
Hinge size (cumulative inc. width; mm)
0
5
10
15
0
20
40
60
80
Age (years) from hinge increments
JC4
B
Shell height from orig. of growth (mm)
0
20
40
60
0
5
10
15
20
Age (years) from oxygen isotope cycles
JC4

NORTH CAROLINA

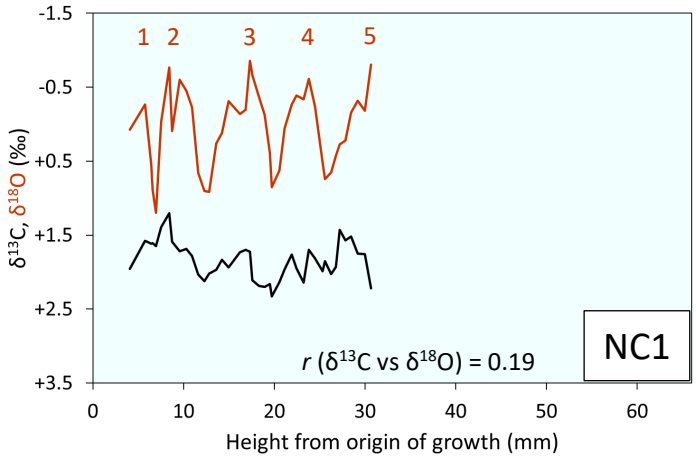

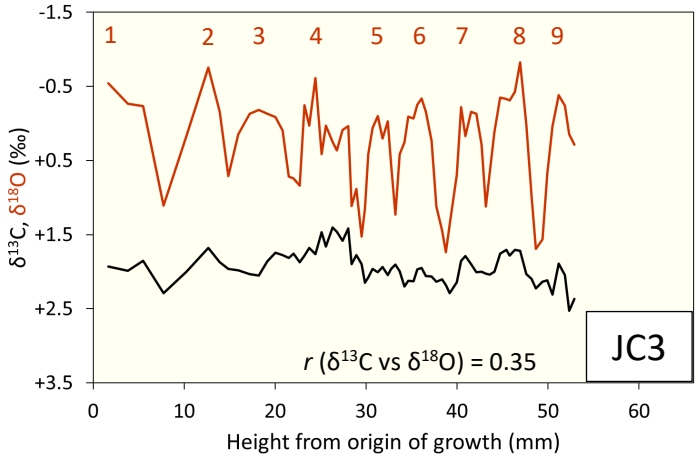

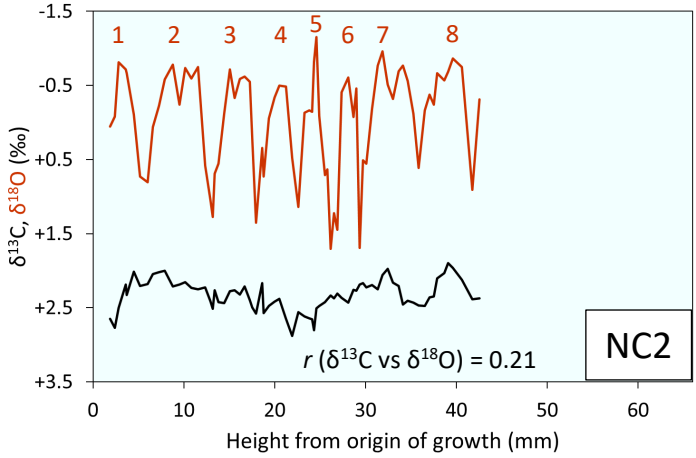

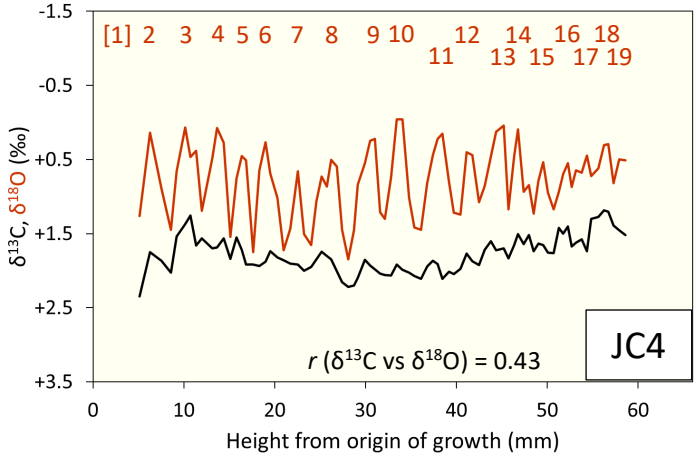

FLORIDA

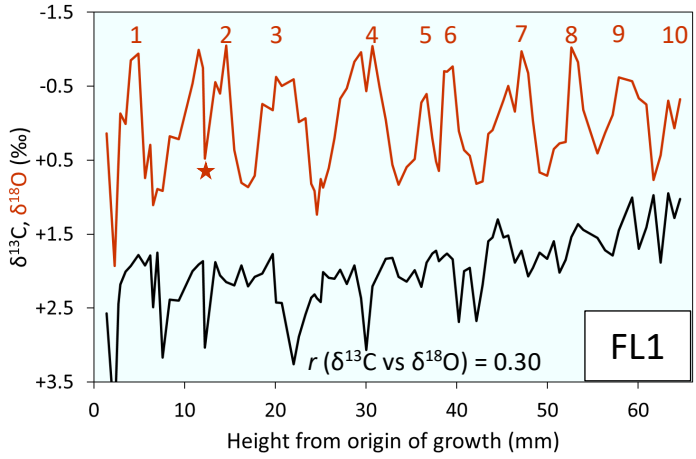

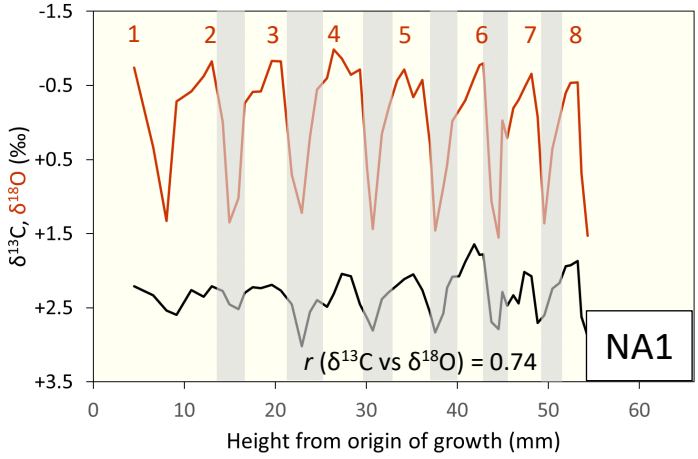

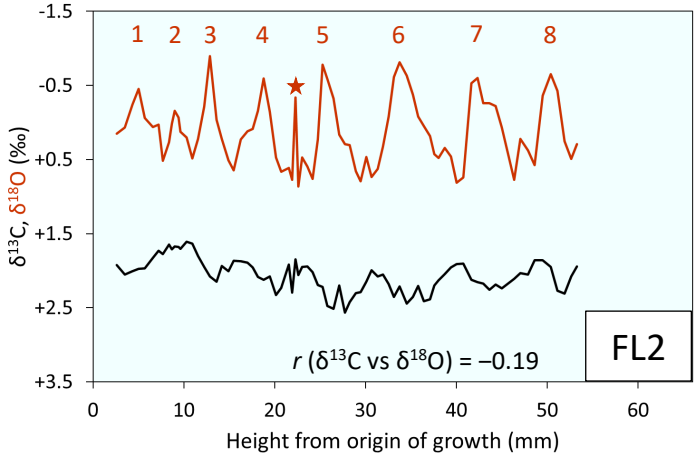

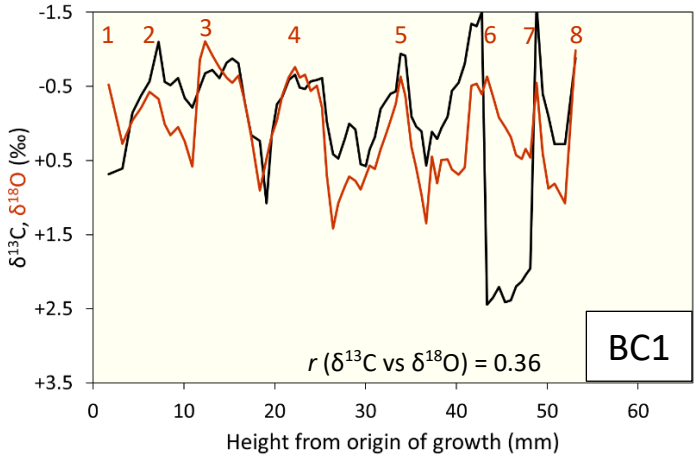

NORTH CAROLINA

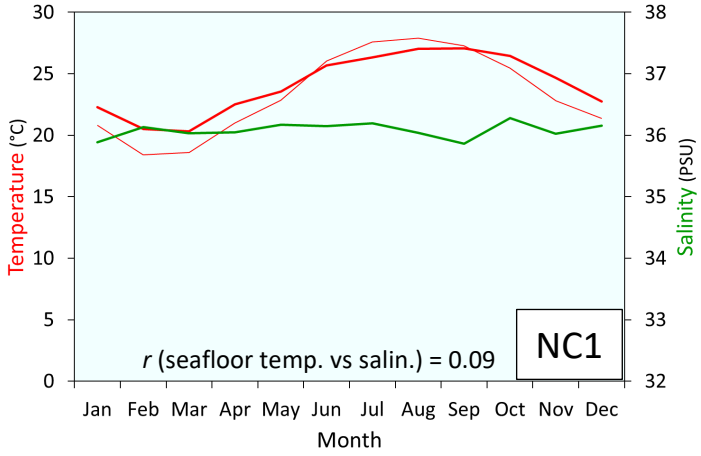

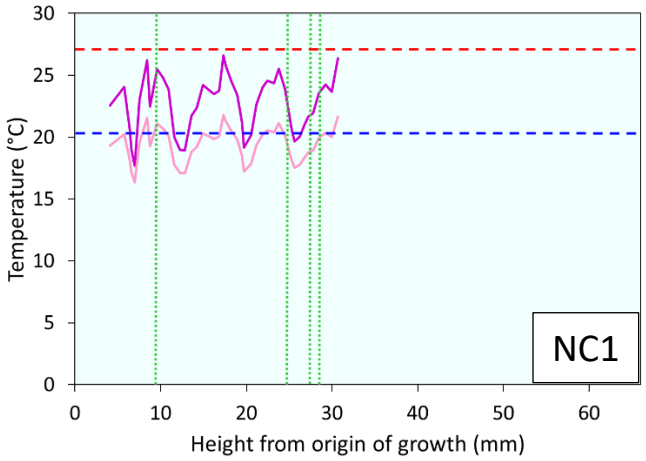

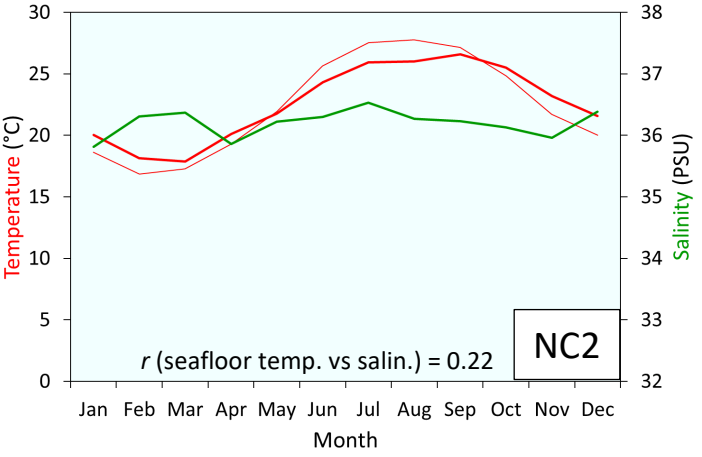

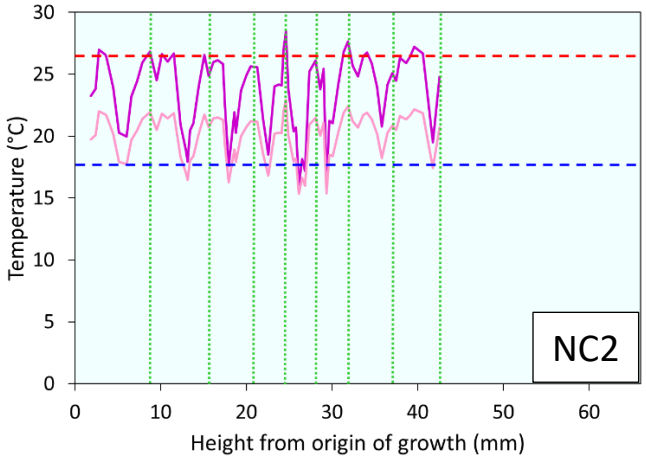

FLORIDA

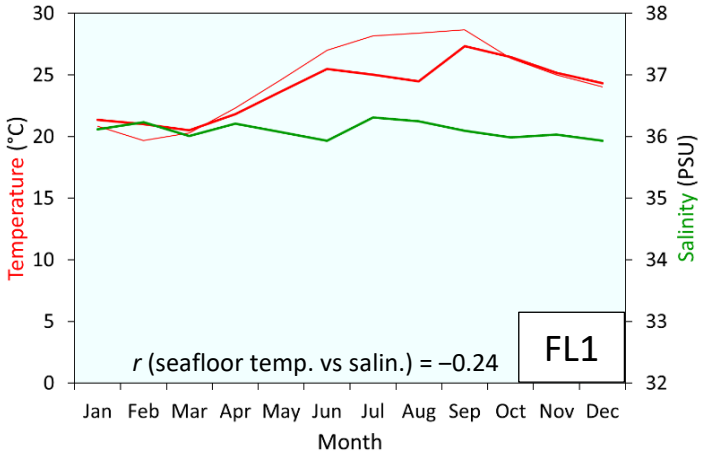

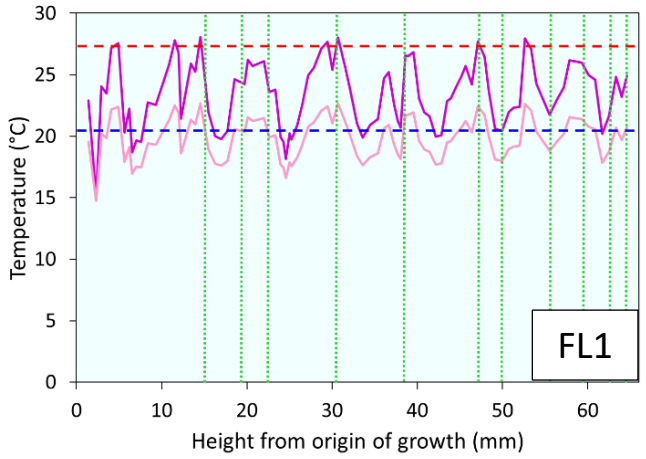

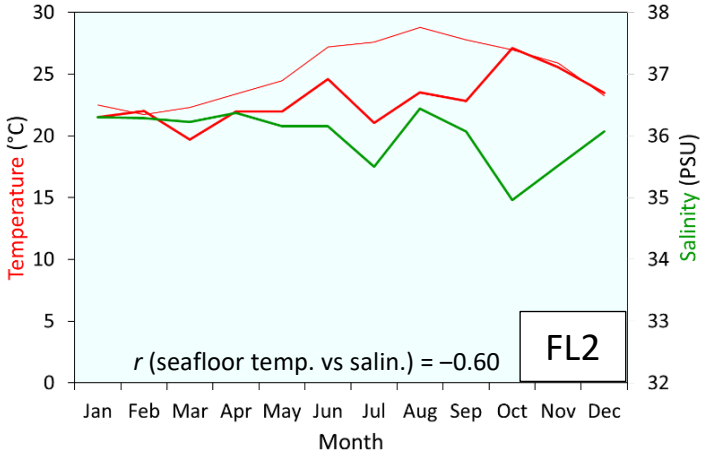

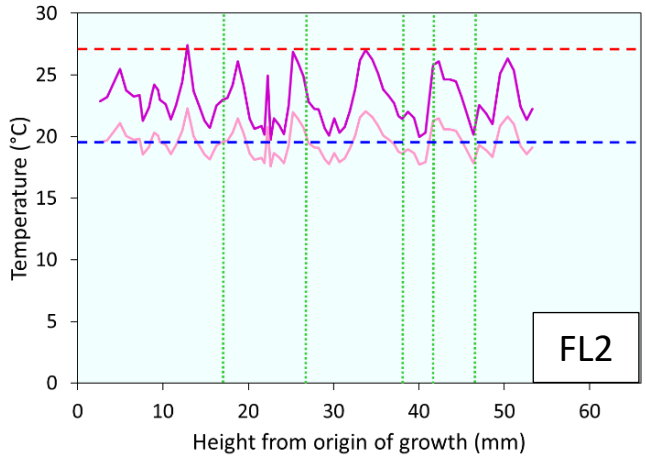

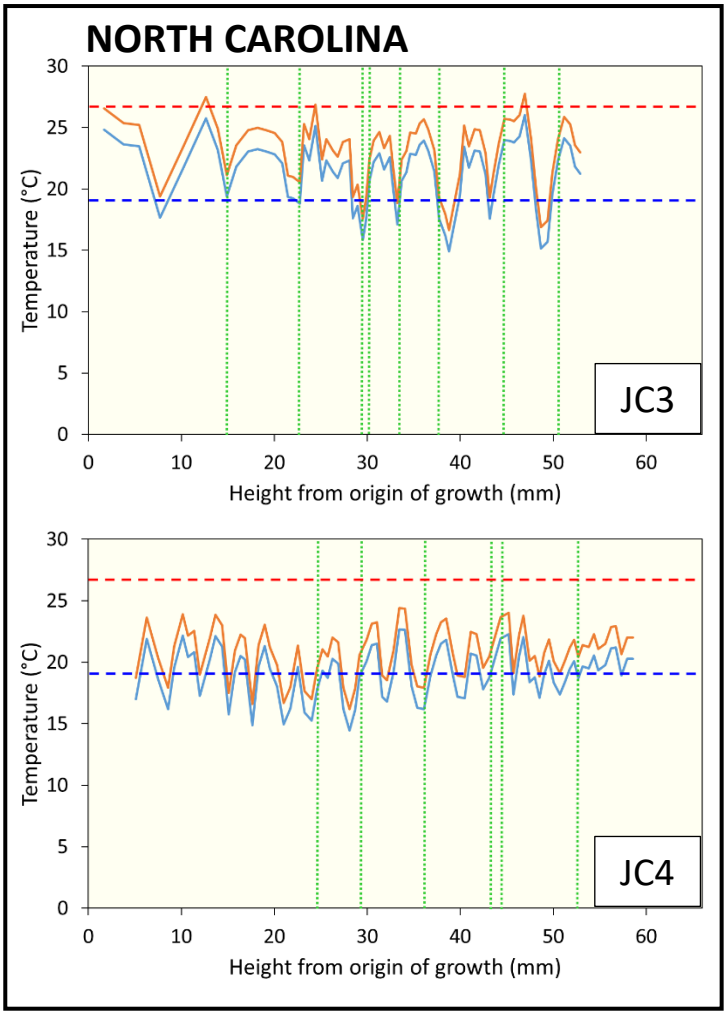
NORTH CAROLINA
Temperature (°C)
Height from origin of growth (mm)
JC3
JC4

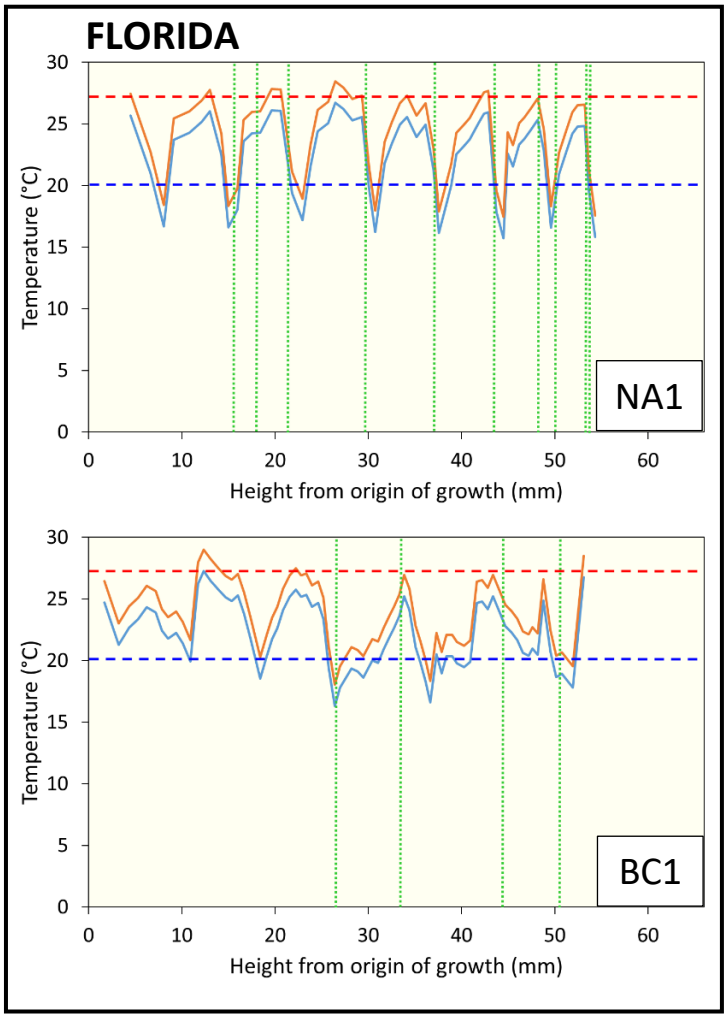
FLORIDA
Temperature (°C)
Height from origin of growth (mm)
NA1
BC1

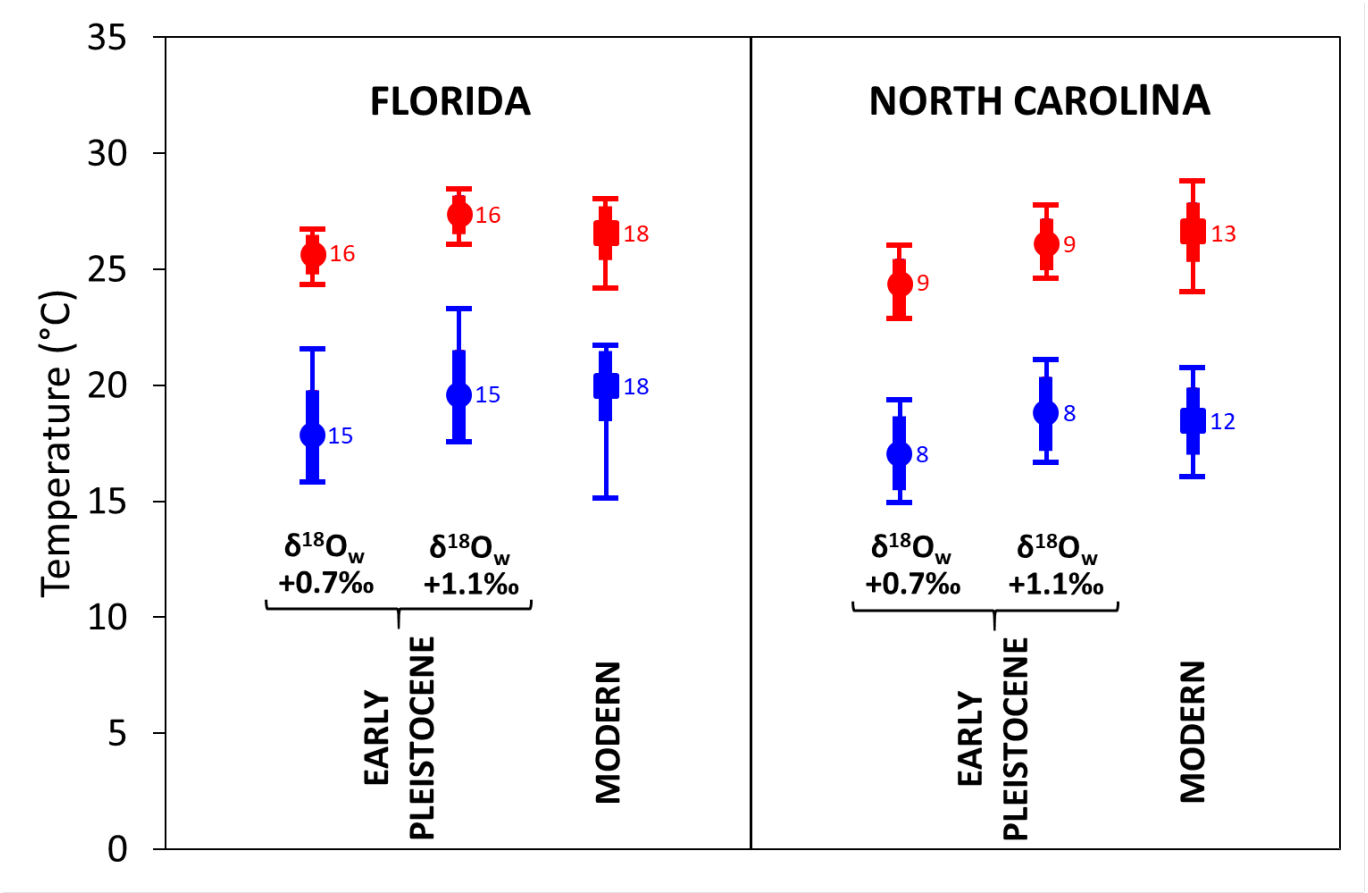
Temperature (°C)
35
30
25
20
15
10
5
0
FLORIDA
NORTH CAROLINA
16
15
16
15
18
18
9
8
9
8
13
12
δ18Ow +0.7‰
δ18Ow +1.1‰
EARLY PLEISTOCENE
MODERN
δ18Ow +0.7‰
δ18Ow +1.1‰
EARLY PLEISTOCENE
MODERN

Code herein	Repository number (valves in lot)	General location	Latitude, longitude	Depth	Date of collection	Valve information	Likely state on collection	Size (length)
NC1	USNM[a] 765110 (6)	Off Ocracoke Inlet, NC	34.70° N, –75.90° E	37 m	December 7th 1961	Disarticulated left valve of pair	Live	37 mm
NC2	USNM[a] 603853 (3)	22 miles SSE of New River Inlet, NC	34.23° N, –77.08° E	27 m[d]	September 8th 1913	Unassociated right valve	Dead	55 mm
FL1	USNM[a] 765112 (1)	25 miles E of St Augustine, FL	29.83° N, –80.88° E	24.7–26.5 m	October 7th 1962	Unassociated right valve[e]	Dead	74 mm[f]
FL2	UF[b] 458113 (2)	Cape Canaveral, FL	*c.* 28.32° N, –80.20° E[c]	*c.* 30–50 m[c]	Unknown	Unassociated left valve	Dead	91 mm

Code herein	Repository number (valves in sample/lot)	General location	Latitude, longitude	Formation	Pleistocene stage	Valve information	Size (length)
JC3[a]	UD[b] 53386 (10[d])	Lee Creek Mine, Aurora, NC	35.37° N, –76.80° E	James City	Calabrian[e]	Disarticulated right valve of probable pair[h]	87 mm
JC4[a]	UD[b] 53387 (10[d])	Lee Creek Mine, Aurora, NC	35.37° N, –76.80° E	James City	Calabrian[e]	Unassociated left valve	81 mm
NA1	UD[b] 53427 (7)	East Coast Aggregates Pit, Hastings, FL	29.68° N, –81.52° E	Nashua	Gelasian[f]	Unassociated left valve	68 mm
BC1	UF[c] 64894 (1)	Star Ranch, Belle Glade, FL	26.70° N, –80.67° E	Bermont/ Caloosahatchee	Calabrian/ Gelasian[g]	Unassociated left valve	84 mm

			Estimated age in years	
			From hinge/ main-shell bands	From $\delta^{18}O$ cycles
Modern	North Carolina	NC1	4	5
		NC2	9	8
	Florida	FL1	10	10
		FL2	*6 (12)*	*8 (11)*
Early Pleistocene	North Carolina	JC3	31	*9 (16)*
		JC4	86	*19 (38)*
	Florida	NA1	*6 (9)*	*8 (9)*
		BC1	15	*8 (10)*

Environmental data: location of NC1

	Surface temp (°C)	Seafloor temp. (°C)	Seafloor salin. (PSU)
Jan	20.80	22.28	35.88
Feb	18.41	20.50	36.13
Mar	18.59	20.32	36.03
Apr	21.01	22.50	36.05
May	22.84	23.54	36.17
Jun	26.03	25.69	36.15
Jul	27.57	26.33	36.20
Aug	27.89	27.02	36.04
Sep	27.26	27.05	35.86
Oct	25.47	26.46	36.28
Nov	22.81	24.66	36.02
Dec	21.39	22.76	36.15

Shell isotope data and calc

Height (mm)	$\delta^{13}C$ (‰)	$\delta^{18}O$ (‰)
4.05	+1.95	+0.07
5.73	+1.58	-0.27
6.40	+1.62	+0.54
6.60	+1.61	+0.89
6.96	+1.65	+1.20
7.50	+1.39	-0.03
8.40	+1.20	-0.77
8.73	+1.59	+0.09
9.56	+1.72	-0.60
10.28	+1.68	-0.45
10.92	+1.78	-0.23
11.60	+2.03	+0.66
12.26	+2.12	+0.90
12.82	+2.02	+0.91
13.58	+1.97	+0.26
14.21	+1.84	+0.12
14.94	+1.94	-0.31
16.20	+1.73	-0.14
16.84	+1.70	-0.20
17.30	+1.73	-0.86
17.58	+2.11	-0.67
18.28	+2.18	-0.37
18.95	+2.20	-0.12
19.50	+2.16	+0.40
19.70	+2.33	+0.85
20.56	+2.14	+0.63
21.14	+1.96	+0.06
21.89	+1.77	-0.27
22.46	+1.95	-0.39
23.21	+2.14	-0.34
23.80	+1.70	-0.61
24.50	+1.82	-0.24
25.30	+1.99	+0.52
25.60	+1.85	+0.74
26.25	+2.03	+0.65
26.78	+1.93	+0.43
27.22	+1.43	+0.27
27.81	+1.57	+0.22
28.45	+1.52	-0.16
29.21	+1.75	-0.32
29.96	+1.76	-0.19
30.67	+2.22	-0.81

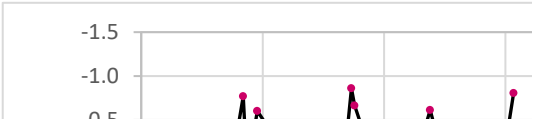

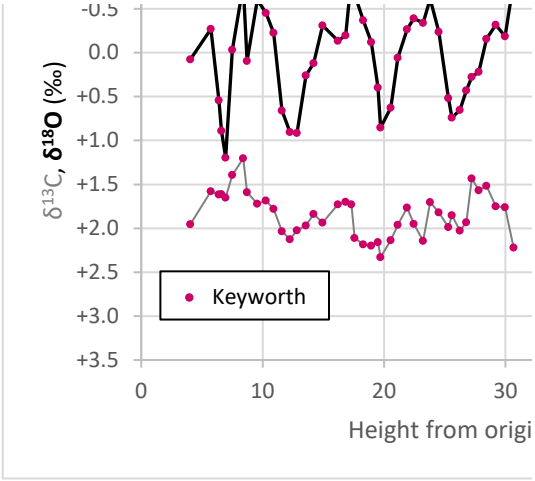
-0.5
0.0
+0.5
+1.0
+1.5
+2.0
+2.5
+3.0
+3.5
δ13C, δ18O (‰)
Keyworth
0
10
20
30
Height from origi

NC1

ulated temperatures ($\delta^{18}O_w$ = +0.7940‰): NC1		Size/cum	
Temp. (°C; Grossman and Ku)	Temp. (°C; Royer et al.)	Year	Inc. width (μm)
22.55	19.31	1	1047.92
24.04	20.22	2	624.28
20.53	18.06	3	1131.27
19.02	17.14	4	1279.48
17.69	16.32	5	1178.43
23.02	19.59		
26.22	21.55		
22.47	19.26		
25.48	21.10		
24.84	20.71		
23.86	20.11		
20.02	17.75		
18.95	17.10		
18.91	17.07		
21.76	18.82		
22.35	19.18		
24.21	20.33		
23.47	19.87		
23.73	20.03		
26.61	21.79		
25.76	21.28		
24.48	20.49		
23.41	19.83		
21.15	18.45		
19.17	17.23		
20.16	17.84		
22.62	19.35		
24.03	20.21		
24.57	20.54		
24.35	20.41		
25.53	21.13		
23.91	20.14		
20.63	18.13		
19.66	17.53		
20.04	17.77		
21.01	18.36		
21.68	18.77		
21.92	18.92		
23.56	19.93		
24.26	20.35		
23.68	20.00		
26.37	21.65		

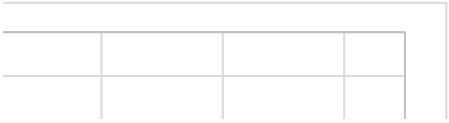

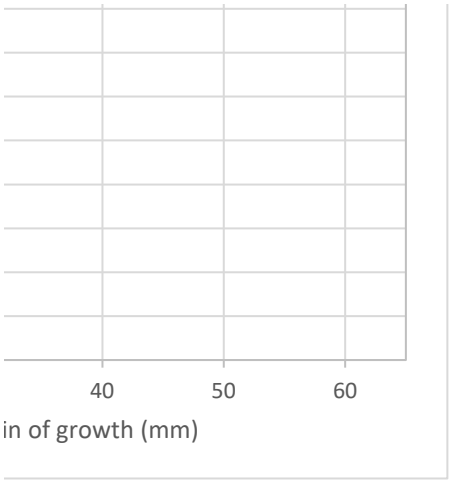
40
50
60
in of growth (mm)

ıulative size of hinge increments: NC1

Cumulative inc. width (µm)	Cumulative inc. width (mm)
1047.92	1.05
1672.20	1.67
2803.47	2.80
4082.95	4.08
5261.38	5.26

Summer $\delta^{18}O$ height: NC1

Year	Height (mm)
1	5.73
2	8.40
3	17.30
4	23.80
5	30.67

Environmental data: location of NC2

	Surface temp (°C)	Seafloor temp. (°C)	Seafloor salin. (PSU)
Jan	18.64	20.03	35.82
Feb	16.86	18.15	36.30
Mar	17.27	17.85	36.37
Apr	19.29	20.10	35.86
May	21.92	21.78	36.22
Jun	25.66	24.31	36.30
Jul	27.55	25.91	36.53
Aug	27.75	25.99	36.27
Sep	27.15	26.59	36.23
Oct	24.82	25.49	36.13
Nov	21.69	23.20	35.96
Dec	20.03	21.56	36.38

Shell isotope data and calc

Height (mm)	$\delta^{13}C$ (‰)	$\delta^{18}O$ (‰)
1.87	+2.65	+0.05
2.40	+2.77	-0.08
2.82	+2.50	-0.81
3.60	+2.19	-0.71
3.71	+2.33	-0.66
4.48	+2.01	-0.11
5.16	+2.20	+0.73
6.00	+2.18	+0.81
6.60	+2.05	+0.06
7.25	+2.02	-0.22
7.87	+2.00	-0.58
8.78	+2.21	-0.78
9.51	+2.19	-0.24
10.14	+2.15	-0.73
10.81	+2.23	-0.60
11.55	+2.25	-0.75
12.34	+2.22	+0.58
12.90	+2.41	+1.04
13.15	+2.52	+1.28
13.40	+2.26	+0.69
13.79	+2.43	+0.56
14.42	+2.43	-0.12
15.07	+2.28	-0.71
15.60	+2.26	-0.33
16.14	+2.32	-0.59
16.68	+2.21	-0.62
17.25	+2.40	-0.55
17.50	+2.49	+0.21
17.96	+2.58	+1.35
18.60	+2.17	+0.35
18.77	+2.57	+0.73
19.37	+2.48	-0.05
19.99	+2.42	-0.33
20.50	+2.38	-0.50
21.25	+2.65	-0.49
21.92	+2.88	+0.48
22.57	+2.56	+1.14
23.25	+2.62	-0.13
23.78	+2.64	-0.16
24.10	+2.66	-0.14
24.34	+2.80	-0.82
24.60	+2.51	-1.16
24.87	+2.48	-0.09
25.53	+2.43	+0.71
25.80	+2.38	+0.63
26.13	+2.34	+1.70
26.50	+2.38	+1.22

26.87	+2.31	+1.45
27.36	+2.36	-0.40
28.08	+2.43	-0.61
28.64	+2.26	-0.07
29.00	+2.27	-0.46
29.37	+2.19	+1.69
29.70	+2.17	+0.51
30.06	+2.22	+0.56
30.71	+2.19	-0.18
31.34	+2.25	-0.77
31.88	+2.06	-0.96
32.43	+1.98	-0.51
33.02	+2.16	-0.32
33.61	+2.21	-0.69
34.08	+2.46	-0.76
34.63	+2.41	-0.56
35.27	+2.43	-0.12
35.81	+2.47	+0.62
36.49	+2.47	-0.16
37.01	+2.36	-0.37
37.50	+2.35	-0.24
37.89	+2.10	-0.66
38.65	+2.03	-0.57
39.07	+1.90	-0.68
39.59	+1.96	-0.86
40.60	+2.12	-0.75
41.75	+2.39	+0.91
42.55	+2.37	-0.31

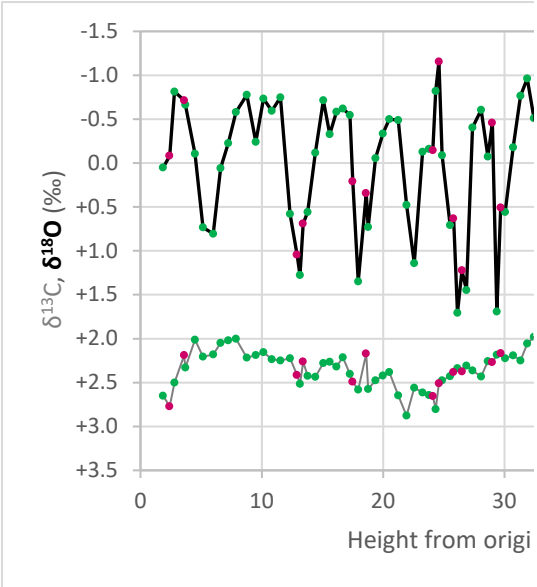

NC2

ulated temperatures ($\delta^{18}O_w$ = +0.9277‰): NC2

Temp. (°C; Grossman and Ku)	Temp. (°C; Royer et al.)
23.23	19.72
23.81	20.08
26.99	22.03
26.55	21.76
26.34	21.63
23.92	20.14
20.28	17.91
19.95	17.71
23.20	19.70
24.43	20.46
25.96	21.40
26.83	21.93
24.50	20.50
26.64	21.81
26.04	21.44
26.70	21.85
20.94	18.32
18.92	17.08
17.92	16.47
20.46	18.03
21.03	18.37
23.97	20.17
26.55	21.76
24.88	20.73
25.99	21.42
26.14	21.51
25.82	21.31
22.54	19.30
17.60	16.27
21.95	18.94
20.28	17.92
23.69	20.00
24.91	20.75
25.62	21.19
25.57	21.16
21.39	18.59
18.50	16.82
24.02	20.20
24.16	20.29
24.08	20.24
27.01	22.04
28.47	22.93
23.83	20.09
20.38	17.98
20.72	18.18
16.06	15.32
18.14	16.60

Size/cum

Year	Inc. width (µm)
1	1483.76
2	755.14
3	534.68
4	636.98
5	544.10
6	499.26
7	544.66
8	688.08
9	554.74
10	432.73

17.18	16.01
25.21	20.94
26.08	21.47
23.77	20.05
25.43	21.07
16.12	15.36
21.25	18.51
21.04	18.38
24.24	20.34
26.78	21.90
27.63	22.42
25.67	21.22
24.82	20.70
26.45	21.70
26.77	21.89
25.89	21.35
23.98	20.18
20.78	18.22
24.16	20.29
25.08	20.86
24.49	20.49
26.32	21.62
25.91	21.36
26.42	21.67
27.21	22.16
26.69	21.85
19.50	17.43
24.80	20.68

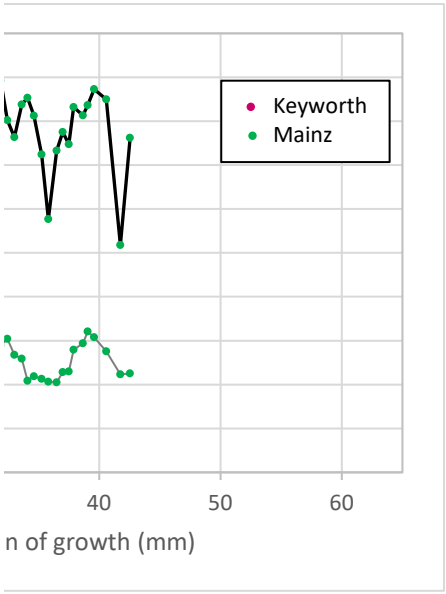

ıulative size of hinge increments: NC2

Cumulative inc. width (µm)	Cumulative inc. width (mm)
1483.76	1.48
2238.89	2.24
2773.57	2.77
3410.56	3.41
3954.65	3.95
4453.91	4.45
4998.58	5.00
5686.65	5.69
6241.39	6.24
6674.12	6.67

Summer $\delta^{18}O$ height: NC2

Year	Height (mm)
1	2.82
2	8.78
3	15.07
4	20.50
5	24.60
6	28.08
7	31.88
8	39.59

Environmental data: location of FL1			
	Surface temp (°C)	Seafloor temp. (°C)	Seafloor salin. (PSU)
Jan	20.82	21.37	36.12
Feb	19.67	20.99	36.23
Mar	20.29	20.50	36.01
Apr	22.31	21.82	36.21
May	24.60	23.68	36.07
Jun	26.99	25.47	35.93
Jul	28.18	25.04	36.31
Aug	28.39	24.49	36.25
Sep	28.65	27.32	36.09
Oct	26.34	26.46	35.98
Nov	25.01	25.16	36.03
Dec	24.04	24.33	35.93

Shell isotope data and calc		
Height (mm)	$\delta^{13}C$ (‰)	$\delta^{18}O$ (‰)
1.42	+2.57	+0.14
2.29	+4.10	+1.93
2.73	+2.45	+0.53
2.91	+2.18	-0.13
3.50	+2.00	+0.01
4.08	+1.93	-0.85
4.90	+1.78	-0.94
5.63	+1.92	+0.74
6.20	+1.79	+0.29
6.50	+2.49	+1.11
7.00	+1.75	+0.89
7.57	+3.17	+0.92
8.36	+2.38	+0.18
9.33	+2.40	+0.22
10.88	+2.00	-0.54
11.56	+1.91	-0.99
12.00	+1.87	-0.75
12.25	+3.04	+0.48
13.40	+1.88	-0.56
13.92	+2.06	-0.40
14.56	+2.15	-1.05
15.48	+2.19	+0.36
16.27	+1.92	+0.80
16.99	+2.21	+0.86
17.72	+2.08	+0.71
18.57	+2.03	-0.26
19.70	+1.77	-0.17
20.10	+2.42	-0.63
20.69	+2.43	-0.51
21.99	+3.26	-0.60
22.60	+2.89	-0.02
23.34	+2.59	-0.07
23.96	+2.36	+0.82
24.30	+2.32	+0.92
24.58	+2.37	+1.23
25.00	+2.42	+0.76
25.25	+2.02	+0.87
25.90	+2.09	+0.60
26.53	+2.10	+0.20
27.15	+1.98	-0.33
27.86	+2.17	-0.47
28.71	+1.93	-0.83
29.44	+2.37	-0.96
30.01	+3.07	-0.44
30.71	+2.21	-1.04
31.50	+2.01	-0.49
32.14	+1.83	-0.05

32.90	+1.82	+0.56
33.57	+2.08	+0.83
34.48	+2.14	+0.59
35.35	+1.99	+0.48
36.07	+2.21	-0.28
36.66	+1.89	-0.39
37.28	+1.76	+0.20
37.70	+1.72	+0.52
38.03	+1.87	+0.65
38.60	+1.79	-0.70
38.90	+1.76	-0.70
39.52	+1.84	-0.77
40.23	+2.69	+0.10
40.80	+2.00	+0.37
41.44	+1.95	+0.44
42.17	+2.68	+0.82
42.84	+2.19	+0.79
43.48	+1.60	+0.15
43.96	+1.54	+0.10
44.49	+1.30	-0.10
45.14	+1.55	-0.31
45.68	+1.52	-0.51
46.39	+1.89	-0.16
47.13	+1.73	-0.97
47.88	+2.07	-0.68
48.40	+1.95	-0.03
49.12	+1.75	+0.67
49.96	+1.84	+0.71
50.70	+1.60	+0.35
51.30	+2.02	+0.28
52.02	+1.85	+0.25
52.62	+1.54	-1.03
53.33	+1.36	-0.83
53.95	+1.45	-0.18
55.51	+1.55	+0.41
56.35	+1.72	+0.13
57.17	+1.79	-0.11
57.83	+1.45	-0.62
59.32	+1.01	-0.57
60.06	+1.70	-0.34
60.88	+1.41	-0.25
61.67	+0.97	+0.76
62.48	+1.88	+0.43
63.28	+0.95	-0.31
63.96	+1.28	+0.07
64.60	+1.02	-0.32

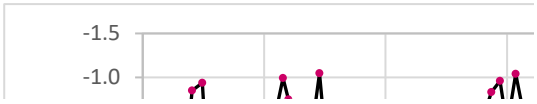

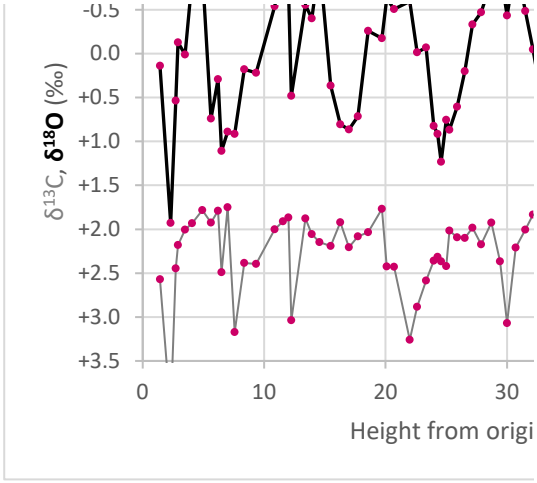
-0.5
0.0
+0.5
+1.0
+1.5
+2.0
+2.5
+3.0
+3.5
δ13C, δ18O (‰)
0
10
20
30
Height from origi

FL1

:ulated temperatures ($\delta^{18}O_w$ = +0.9402‰): FL1

Temp. (°C; Grossman and Ku)	Temp. (°C; Royer et al.)
22.91	19.53
15.13	14.76
21.19	18.47
24.07	20.23
23.46	19.86
27.20	22.15
27.58	22.39
20.30	17.93
22.24	19.12
18.70	16.95
19.65	17.53
19.53	17.45
22.74	19.42
22.57	19.32
25.85	21.33
27.81	22.53
26.75	21.88
21.43	18.62
25.92	21.37
25.25	20.96
28.05	22.68
21.93	18.92
20.02	17.75
19.77	17.60
20.42	18.00
24.64	20.59
24.27	20.36
26.23	21.56
25.71	21.24
26.10	21.48
23.58	19.94
23.80	20.07
19.94	17.71
19.54	17.46
18.16	16.61
20.23	17.88
19.74	17.58
20.89	18.29
22.64	19.36
24.95	20.78
25.54	21.14
27.12	22.11
27.67	22.44
25.40	21.05
28.02	22.66
25.62	21.19
23.72	20.02

Size/cun

Year	Inc. width (µm)
1	1402.15
2	1436.07
3	1493.98
4	1199.83
5	1212.18
6	864.25
7	591.71
8	706.81
9	652.83
10	722.17

21.06	18.39
19.89	17.67
20.94	18.32
21.41	18.61
24.73	20.64
25.22	20.94
22.64	19.36
21.25	18.51
20.70	18.17
26.55	21.76
26.53	21.75
26.84	21.94
23.05	19.61
21.92	18.92
21.61	18.73
19.95	17.71
20.09	17.80
22.87	19.50
23.09	19.64
23.93	20.15
24.85	20.71
25.70	21.24
24.20	20.32
27.72	22.48
26.45	21.70
23.65	19.98
20.62	18.12
20.43	18.01
21.99	18.96
22.31	19.16
22.41	19.22
27.96	22.62
27.10	22.09
24.30	20.38
21.73	18.80
22.94	19.54
23.99	20.19
26.19	21.53
25.97	21.40
24.97	20.79
24.61	20.57
20.19	17.86
21.62	18.74
24.84	20.71
23.21	19.71
24.91	20.75

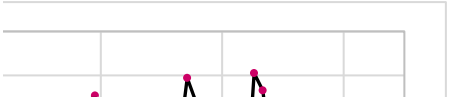

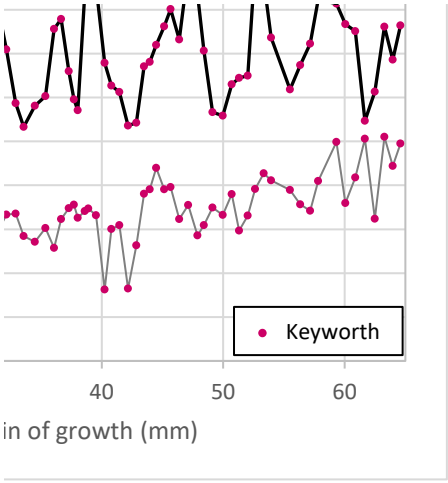
Keyworth
40
50
60
in of growth (mm)

ılulative size of hinge increments: FL1

Cumulative inc. width (µm)	Cumulative inc. width (mm)
1402.15	1.40
2838.23	2.84
4332.21	4.33
5532.04	5.53
6744.22	6.74
7608.46	7.61
8200.18	8.20
8906.99	8.91
9559.82	9.56
10281.99	10.28

Summer $\delta^{18}O$ height: FL1

Year	Height (mm)
1	4.90
2	14.56
3	20.10
4	30.71
5	36.66
6	39.52
7	47.13
8	52.62
9	57.83
10	64.60

Environmental data: location of FL2

	Surface temp (°C)	Seafloor temp. (°C)	Seafloor salin. (PSU)
Jan	22.51	21.51	36.30
Feb	21.71	22.03	36.29
Mar	22.30	19.69	36.22
Apr	23.37	21.96	36.37
May	24.46	21.96	36.15
Jun	27.20	24.60	36.16
Jul	27.58	21.06	35.50
Aug	28.80	23.52	36.44
Sep	27.78	22.81	36.07
Oct	26.95	27.10	34.96
Nov	25.90	25.55	35.52
Dec	23.27	23.50	36.07

Shell isotope data and calc

Height (mm)	$\delta^{13}C$ (‰)	$\delta^{18}O$ (‰)
2.63	+1.92	+0.15
3.49	+2.05	+0.07
4.35	+2.01	-0.24
4.99	+1.98	-0.45
5.72	+1.97	-0.06
6.57	+1.83	+0.06
7.23	+1.73	+0.03
7.66	+1.78	+0.51
8.39	+1.65	+0.27
8.70	+1.71	+0.01
8.98	+1.67	-0.16
9.40	+1.68	-0.07
9.62	+1.71	+0.13
10.30	+1.61	+0.20
10.92	+1.63	+0.49
11.56	+1.80	+0.22
12.24	+1.95	-0.22
12.84	+2.08	-0.90
13.59	+2.15	-0.04
14.20	+1.94	+0.22
14.89	+2.01	+0.51
15.49	+1.87	+0.65
16.26	+1.87	+0.23
16.99	+1.89	+0.12
17.55	+1.95	+0.09
18.16	+2.09	-0.15
18.78	+2.12	-0.59
19.47	+2.08	-0.14
20.16	+2.33	+0.47
20.74	+2.23	+0.66
21.53	+1.92	+0.61
21.90	+2.30	+0.77
22.27	+1.85	-0.33
22.60	+2.06	+0.87
23.00	+1.95	+0.47
23.60	+1.94	+0.59
24.17	+2.02	+0.76
24.72	+2.19	+0.23
25.24	+2.22	-0.78
25.79	+2.47	-0.59
26.46	+2.52	-0.33
27.07	+2.20	+0.16
27.74	+2.56	+0.29
28.26	+2.43	+0.30
28.94	+2.30	+0.66
29.45	+2.29	+0.79
30.06	+2.15	+0.47

30.67	+1.99	+0.74
31.31	+2.08	+0.63
31.93	+2.05	+0.33
32.53	+2.18	-0.08
33.10	+2.35	-0.62
33.74	+2.21	-0.81
34.50	+2.44	-0.63
35.22	+2.35	-0.37
35.78	+2.21	-0.08
36.39	+2.41	+0.05
37.08	+2.39	+0.18
37.58	+2.20	+0.43
38.03	+2.13	+0.48
38.72	+2.05	+0.34
39.40	+1.95	+0.46
40.03	+1.91	+0.81
40.75	+1.91	+0.74
41.66	+2.13	-0.53
42.34	+2.15	-0.60
42.92	+2.17	-0.26
43.63	+2.26	-0.26
44.30	+2.19	-0.22
44.97	+2.24	+0.07
46.37	+2.11	+0.77
47.03	+2.03	+0.22
47.87	+2.05	+0.38
48.59	+1.86	+0.58
49.49	+1.86	-0.36
50.37	+1.95	-0.65
51.10	+2.27	-0.43
51.89	+2.31	+0.25
52.63	+2.08	+0.49
53.26	+1.94	+0.29

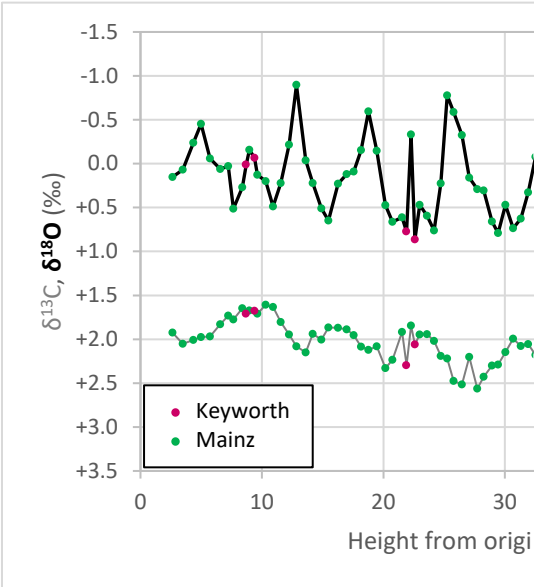

FL2

:ulated temperatures ($\delta^{18}O_w$ = +0.9400‰): FL2

Temp. (°C; Grossman and Ku)	Temp. (°C; Royer et al.)
22.84	19.49
23.21	19.71
24.54	20.53
25.48	21.10
23.76	20.05
23.25	19.73
23.38	19.81
21.27	18.52
22.34	19.18
23.45	19.86
24.20	20.31
23.79	20.07
22.96	19.56
22.64	19.36
21.40	18.60
22.54	19.30
24.45	20.47
27.40	22.28
23.67	19.99
22.54	19.30
21.30	18.54
20.70	18.17
22.52	19.29
22.99	19.58
23.12	19.66
24.18	20.30
26.08	21.47
24.14	20.28
21.45	18.63
20.62	18.12
20.86	18.27
20.15	17.83
24.96	20.78
19.75	17.59
21.46	18.64
20.93	18.31
20.20	17.86
22.53	19.29
26.89	21.96
26.06	21.45
24.92	20.76
22.81	19.46
22.25	19.12
22.19	19.08
20.65	18.14
20.07	17.78
21.47	18.65

Size/cur

Year	Inc. width (µm)
1	1537.80
2	1192.55
3	1181.90
4	868.55
5	908.21
6	944.53
	No

20.31	17.93
20.79	18.22
22.09	19.02
23.85	20.10
26.18	21.53
27.04	22.06
26.26	21.58
25.13	20.89
23.84	20.10
23.30	19.77
22.71	19.40
21.65	18.76
21.42	18.61
22.02	18.98
21.51	18.67
19.98	17.73
20.30	17.93
25.80	21.30
26.10	21.48
24.64	20.59
24.65	20.59
24.48	20.49
23.21	19.71
20.15	17.83
22.54	19.30
21.88	18.89
21.00	18.36
25.09	20.86
26.34	21.63
25.36	21.03
22.42	19.22
21.36	18.58
22.25	19.12

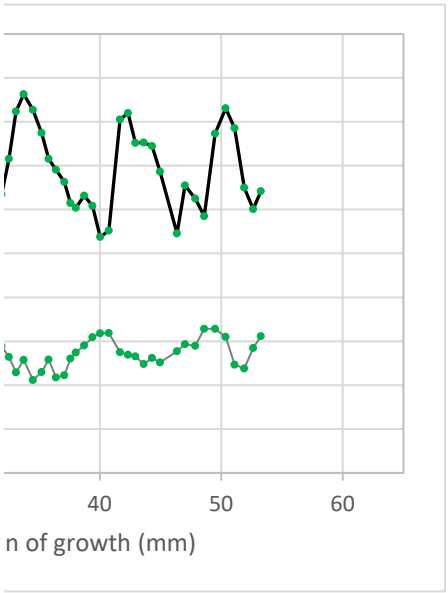

ılulative size of hinge increments: FL2

Cumulative inc. width (µm)	Cumulative inc. width (mm)
1537.80	1.54
2730.35	2.73
3912.25	3.91
4780.80	4.78
5689.01	5.69
6633.54	6.63

ıt to ventral edge of hinge plate

Summer $\delta^{18}O$ height: FL2

Year	Height (mm)
1	4.99
2	8.98
3	12.84
4	18.78
5	25.24
6	33.74
7	42.34
8	50.37

Shell data and calculated temperatures (Grossman and Ku): JC3

Height (mm)	$\delta^{13}C$ (‰)	$\delta^{18}O$ (‰)	Temp. ($\delta^{18}O_w$ = +0.7‰): JC3	Temp. ($\delta^{18}O_w$ = +1.1‰): JC3
1.69	+1.93	-0.54	24.82	26.56
3.80	+1.99	-0.27	23.62	25.36
5.48	+1.85	-0.23	23.47	25.21
7.71	+2.29	+1.11	17.67	19.41
10.22	+2.00	+0.17	21.72	23.45
12.64	+1.68	-0.75	25.74	27.47
13.93	+1.87	-0.16	23.15	24.89
14.87	+1.96	+0.71	19.38	21.11
15.93	+1.98	+0.15	21.83	23.56
17.19	+2.03	-0.13	23.03	24.77
18.22	+2.05	-0.18	23.25	24.98
19.12	+1.86	-0.13	23.05	24.79
20.01	+1.74	-0.08	22.83	24.57
20.84	+1.77	+0.09	22.07	23.81
21.48	+1.82	+0.72	19.36	21.09
22.02	+1.76	+0.74	19.23	20.97
22.71	+1.87	+0.84	18.83	20.56
23.20	+1.78	-0.25	23.54	25.28
23.76	+1.68	+0.03	22.33	24.06
24.40	+1.76	-0.62	25.14	26.87
25.12	+1.47	+0.42	20.66	22.40
25.58	+1.66	+0.03	22.33	24.07
26.29	+1.40	+0.25	21.38	23.12
26.79	+1.46	+0.36	20.90	22.63
27.39	+1.59	+0.08	22.10	23.84
28.06	+1.42	+0.04	22.30	24.04
28.42	+1.90	+1.12	17.62	19.36
28.95	+1.77	+0.88	18.63	20.37
29.51	+1.90	+1.53	15.84	17.58
29.86	+2.15	+1.15	17.48	19.22
30.24	+2.08	+0.41	20.67	22.41
30.70	+1.96	+0.06	22.19	23.93
31.27	+2.01	-0.10	22.89	24.63
31.79	+1.93	+0.20	21.60	23.33
32.39	+2.05	-0.03	22.60	24.34
32.77	+1.96	+0.55	20.06	21.80
33.22	+1.91	+1.23	17.13	18.87
33.67	+2.00	+0.42	20.66	22.39
34.19	+2.20	+0.26	21.36	23.09
34.62	+2.12	-0.09	22.86	24.60
35.19	+2.13	-0.07	22.77	24.50
35.64	+1.97	-0.26	23.58	25.32
36.07	+1.95	-0.34	23.94	25.68
36.56	+2.06	-0.16	23.14	24.88
37.21	+2.07	+0.24	21.44	23.18
37.72	+2.13	+1.12	17.59	19.32
38.35	+2.10	+1.44	16.22	17.95

38.77	+2.18	+1.74	14.93	16.67
39.20	+2.29	+1.37	16.54	18.28
39.94	+2.14	+0.69	19.46	21.19
40.43	+1.86	-0.22	23.43	25.17
40.92	+1.79	+0.17	21.73	23.46
41.52	+1.90	-0.16	23.15	24.88
42.10	+2.01	-0.13	23.03	24.77
42.68	+2.00	+0.29	21.22	22.95
43.15	+2.03	+1.12	17.59	19.33
43.57	+2.04	+0.67	19.55	21.28
44.12	+2.00	+0.11	21.97	23.70
44.72	+1.76	-0.35	23.99	25.72
45.39	+1.71	-0.33	23.91	25.65
45.77	+1.78	-0.31	23.80	25.54
46.35	+1.71	-0.42	24.31	26.04
46.93	+1.72	-0.82	26.04	27.77
47.58	+2.03	+0.02	22.38	24.12
48.17	+2.10	+0.98	18.21	19.95
48.65	+2.23	+1.69	15.13	16.86
49.38	+2.14	+1.56	15.68	17.42
49.89	+2.12	+0.68	19.53	21.27
50.48	+2.31	+0.04	22.31	24.05
51.16	+1.89	-0.38	24.12	25.85
51.84	+2.05	-0.24	23.50	25.23
52.32	+2.53	+0.15	21.83	23.57
52.90	+2.37	+0.29	21.23	22.96

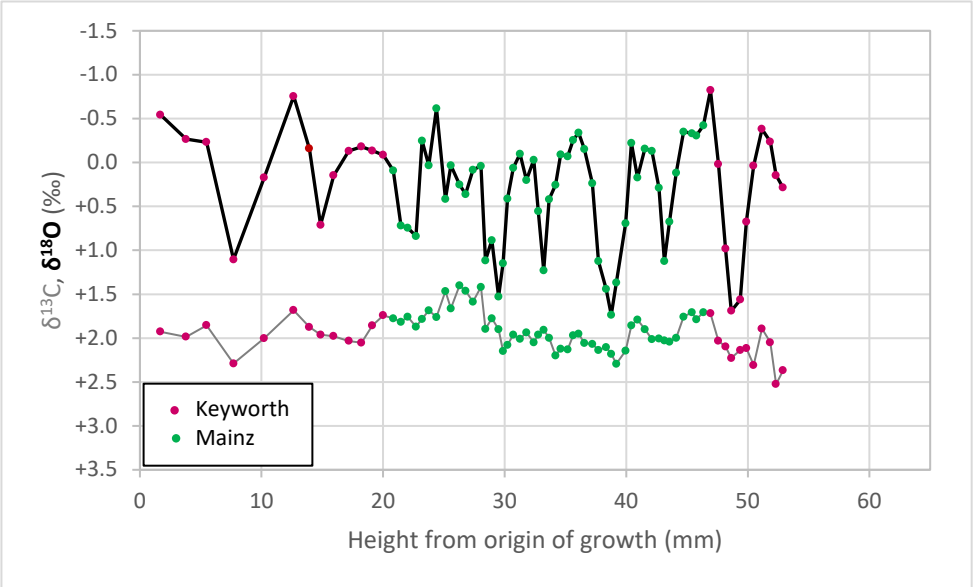

JC3

Size/cumulative size of hinge increments: JC3

Year	Inc. width (µm)	Cumulative inc. width (µm)	Cumulative inc. width (mm)
1	596.56	596.56	0.60
2	634.11	1230.67	1.23
3	718.90	1949.57	1.95
4	447.99	2397.56	2.40
5	431.52	2829.08	2.83
6	398.20	3227.27	3.23
7	350.96	3578.23	3.58
8	348.72	3926.95	3.93
9	168.96	4095.91	4.10
10	250.50	4346.41	4.35
11	369.42	4715.83	4.72
12	345.23	5061.06	5.06
13	297.64	5358.70	5.36
14	297.08	5655.78	5.66
15	345.23	6001.01	6.00
16	289.80	6290.81	6.29
17	482.56	6773.37	6.77
18	455.35	7228.72	7.23
19	352.58	7581.30	7.58
20	242.11	7823.41	7.82
21	227.86	8051.26	8.05
22	242.11	8293.37	8.29
23	200.94	8494.31	8.49
24	172.85	8667.16	8.67
25	139.38	8806.55	8.81
26	124.25	8930.80	8.93
27	179.33	9110.13	9.11
28	144.90	9255.03	9.26
29	144.90	9399.92	9.40
30	110.49	9510.41	9.51
31	89.86	9600.28	9.60
32	82.71	9682.98	9.68

Summer $\delta^{18}O$ height: JC3

Year	Height (mm)
1	1.69
2	12.64
3	18.22
4	24.4
5	31.27
6	36.07
7	40.43
8	46.93
9	51.16

Shell data and calculated temperatures (Grossman and Ku): JC4

Height (mm)	$\delta^{13}C$ (‰)	$\delta^{18}O$ (‰)	Temp. ($\delta^{18}O_w$ = +0.7‰): JC4	Temp. ($\delta^{18}O_w$ = +1.1‰): JC4
5.10	+2.34	+1.26	17.00	18.73
6.26	+1.75	+0.14	21.88	23.61
7.50	+1.86	+0.89	18.61	20.34
8.56	+2.03	+1.45	16.18	17.92
9.22	+1.54	+0.66	19.60	21.34
10.15	+1.37	+0.07	22.17	23.90
10.71	+1.26	+0.47	20.43	22.17
11.35	+1.66	+0.38	20.80	22.54
11.98	+1.57	+1.19	17.28	19.02
13.10	+1.70	+0.49	20.36	22.09
13.64	+1.69	+0.08	22.14	23.87
14.40	+1.57	+0.28	21.27	23.01
15.11	+1.84	+1.55	15.76	17.49
15.77	+1.55	+0.75	19.20	20.94
16.38	+1.72	+0.45	20.49	22.23
16.84	+1.91	+0.51	20.25	21.99
17.64	+1.92	+1.75	14.88	16.62
18.29	+1.94	+0.64	19.68	21.41
18.96	+1.88	+0.27	21.30	23.04
19.51	+1.74	+0.69	19.47	21.21
20.29	+1.82	+1.02	18.05	19.78
20.99	+1.86	+1.73	14.97	16.71
21.72	+1.90	+1.44	16.22	17.96
22.54	+1.91	+0.66	19.60	21.34
23.24	+2.00	+1.51	15.93	17.67
24.02	+1.95	+1.66	15.28	17.01
24.60	+1.85	+1.06	17.86	19.60
25.17	+1.74	+0.73	19.30	21.03
25.75	+1.80	+0.86	18.72	20.45
26.23	+1.85	+0.51	20.26	22.00
26.84	+2.01	+0.59	19.89	21.63
27.40	+2.16	+1.45	16.19	17.93
28.07	+2.22	+1.84	14.46	16.20
28.70	+2.20	+1.45	16.15	17.89
29.16	+2.09	+0.84	18.84	20.57
29.90	+1.86	+0.55	20.07	21.81
30.47	+1.93	+0.25	21.39	23.12
31.02	+1.98	+0.22	21.50	23.23
31.60	+2.04	+1.21	17.20	18.94
32.12	+2.06	+1.30	16.82	18.55
32.81	+2.07	+0.74	19.25	20.98
33.42	+1.92	-0.04	22.65	24.39
34.04	+1.99	-0.04	22.64	24.38
34.78	+2.02	+1.02	18.05	19.78
35.38	+2.07	+1.42	16.31	18.04
36.08	+2.11	+1.45	16.19	17.92
36.78	+1.94	+0.82	18.91	20.65

37.40	+1.87	+0.44	20.54	22.28
37.94	+1.91	+0.22	21.50	23.24
38.46	+2.11	+0.15	21.82	23.56
39.19	+2.01	+0.81	18.97	20.71
39.70	+2.04	+1.22	17.17	18.91
40.45	+1.97	+1.24	17.07	18.81
41.11	+1.77	+0.40	20.72	22.46
41.76	+1.87	+0.44	20.56	22.30
42.47	+1.92	+1.07	17.80	19.54
43.13	+1.72	+0.86	18.73	20.47
43.80	+1.60	+0.46	20.46	22.19
44.34	+1.73	+0.12	21.93	23.66
45.21	+1.70	+0.04	22.29	24.03
45.72	+1.83	+1.17	17.38	19.11
46.33	+1.65	+0.45	20.51	22.24
46.79	+1.51	+0.10	22.05	23.79
47.42	+1.64	+0.94	18.40	20.14
47.98	+1.52	+0.85	18.79	20.52
48.50	+1.74	+1.23	17.12	18.85
49.04	+1.63	+0.79	19.04	20.77
49.55	+1.65	+0.54	20.13	21.87
50.05	+1.76	+0.95	18.36	20.09
50.68	+1.76	+1.17	17.38	19.12
51.25	+1.42	+0.93	18.42	20.15
51.75	+1.50	+0.70	19.45	21.18
52.25	+1.40	+0.55	20.07	21.81
52.67	+1.67	+0.87	18.70	20.44
53.17	+1.62	+0.65	19.66	21.39
53.80	+1.57	+0.68	19.52	21.26
54.36	+1.74	+0.44	20.54	22.28
54.85	+1.30	+0.72	19.33	21.07
55.59	+1.28	+0.62	19.78	21.51
56.22	+1.19	+0.31	21.14	22.87
56.71	+1.20	+0.30	21.18	22.92
57.31	+1.39	+0.82	18.92	20.66
57.93	+1.46	+0.50	20.29	22.03
58.57	+1.52	+0.51	20.26	22.00

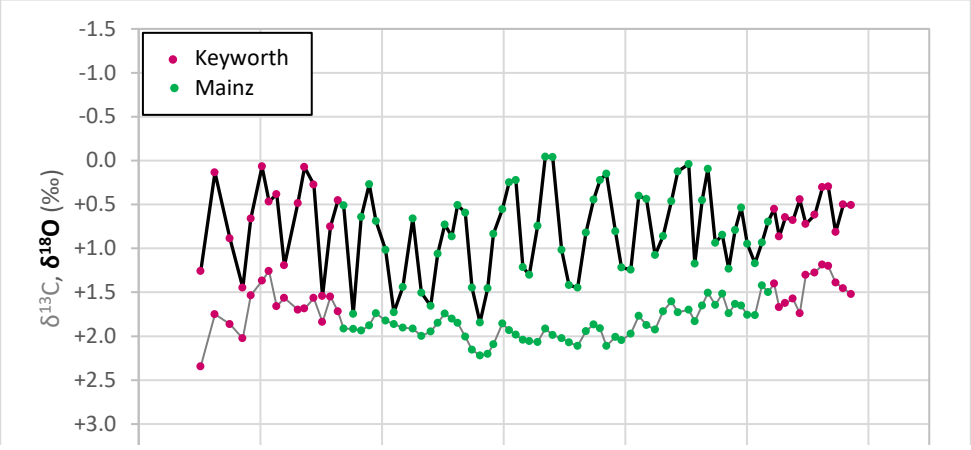

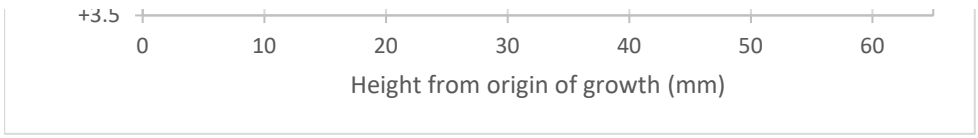
+3.5
0
10
20
30
40
50
60
Height from origin of growth (mm)

JC4

Size/cumulative size of hinge increments: JC4

Year	Inc. width (µm)	Cumulative inc. width (µm)	Cumulative inc. width (mm)
1	1261.87	1261.87	1.26
2	489.56	1751.43	1.75
3	407.00	2158.43	2.16
4	434.18	2592.61	2.59
5	470.62	3063.23	3.06
6	456.48	3519.71	3.52
7	634.34	4154.04	4.15
8	501.11	4655.15	4.66
9	403.08	5058.23	5.06
10	267.22	5325.45	5.33
11	349.02	5674.48	5.67
12	313.09	5987.57	5.99
13	341.66	6329.23	6.33
14	251.66	6580.89	6.58
15	275.21	6856.10	6.86
16	308.51	7164.61	7.16
17	236.62	7401.24	7.40
18	164.45	7565.69	7.57
19	246.88	7812.57	7.81
20	277.69	8090.26	8.09
21	234.46	8324.72	8.32
22	292.33	8617.05	8.62
23	387.01	9004.06	9.00
24	243.12	9247.18	9.25
25	295.24	9542.42	9.54
26	136.51	9678.93	9.68
27	115.77	9794.70	9.79
28	110.02	9904.72	9.90
29	115.77	10020.50	10.02
30	104.24	10124.73	10.12
31	131.76	10256.49	10.26
32	134.00	10390.49	10.39
33	134.00	10524.48	10.52
34	143.31	10667.79	10.67
35	102.81	10770.59	10.77
36	105.97	10876.56	10.88
37	93.46	10970.02	10.97
38	99.74	11069.76	11.07
39	115.31	11185.07	11.19
40	105.92	11290.99	11.29
41	110.78	11401.78	11.40
42	95.86	11497.64	11.50
43	107.67	11605.31	11.61
44	77.96	11683.27	11.68
45	74.98	11758.25	11.76
46	62.86	11821.11	11.82
47	116.64	11937.75	11.94

48	104.81	12042.56	12.04
49	128.70	12171.26	12.17
50	107.67	12278.93	12.28
51	87.65	12366.58	12.37
52	111.42	12478.00	12.48
53	85.10	12563.10	12.56
54	135.26	12698.36	12.70
55	191.18	12889.54	12.89
56	88.41	12977.95	12.98
57	94.65	13072.60	13.07
58	120.46	13193.05	13.19
59	108.54	13301.59	13.30
60	96.63	13398.22	13.40
61	97.86	13496.08	13.50
62	92.92	13589.00	13.59
63	89.36	13678.36	13.68
64	98.32	13776.68	13.78
65	116.91	13893.59	13.89
66	103.13	13996.72	14.00
67	110.20	14106.93	14.11
68	91.96	14198.89	14.20
69	80.42	14279.31	14.28
70	61.81	14341.12	14.34
71	75.96	14417.08	14.42
72	110.20	14527.28	14.53
73	84.89	14612.16	14.61
74	80.67	14692.84	14.69
75	84.72	14777.55	14.78
76	47.73	14825.28	14.83
77	62.18	14887.46	14.89
78	81.01	14968.47	14.97
79	83.02	15051.49	15.05
80	89.07	15140.56	15.14
81	93.44	15234.00	15.23
82	84.72	15318.72	15.32
83	103.22	15421.93	15.42
84	113.63	15535.56	15.54
85	80.39	15615.95	15.62
86	88.76	15704.71	15.70

Summer $\delta^{18}O$ height: JC4

Year [1]	Height (mm)
2	6.26
3	10.15
4	13.64
5	16.38
6	18.96
7	22.54
8	26.23
9	31.02
10	33.42
11	38.46
12	41.11
13	45.21
14	46.79
15	49.55
16	52.25
17	54.36
18	56.71
19	57.93

NA1

Shell data and calculated temperatures (Grossman and Ku): NA1

Height (mm)	$\delta^{13}C$ (‰)	$\delta^{18}O$ (‰)	Temp. ($\delta^{18}O_w$ = +0.7‰): NA1	Temp. ($\delta^{18}O_w$ = +1.1‰): NA1
4.52	+2.21	-0.74	25.69	27.43
6.61	+2.33	+0.34	21.01	22.75
8.04	+2.54	+1.33	16.69	18.43
9.14	+2.59	-0.28	23.70	25.43
10.80	+2.26	-0.42	24.28	26.01
12.12	+2.35	-0.63	25.18	26.91
13.00	+2.21	-0.82	26.04	27.77
14.21	+2.27	-0.01	22.49	24.23
14.98	+2.45	+1.35	16.62	18.35
15.97	+2.52	+1.02	18.05	19.78
16.63	+2.30	-0.26	23.58	25.32
17.52	+2.23	-0.41	24.26	26.00
18.40	+2.23	-0.42	24.30	26.03
19.61	+2.19	-0.83	26.08	27.82
20.60	+2.27	-0.83	26.05	27.78
21.81	+2.46	+0.71	19.40	21.13
22.91	+3.02	+1.22	17.18	18.91
23.79	+2.56	+0.20	21.60	23.33
24.57	+2.39	-0.44	24.38	26.12
25.67	+2.49	-0.60	25.07	26.80
26.44	+2.31	-0.98	26.73	28.47
27.32	+2.04	-0.86	26.22	27.96
28.31	+2.07	-0.65	25.27	27.01
29.30	+2.46	-0.72	25.58	27.31
30.07	+2.64	+0.62	19.76	21.50
30.73	+2.81	+1.44	16.21	17.95
31.73	+2.39	+0.15	21.81	23.55
32.50	+2.29	-0.21	23.39	25.13
33.38	+2.19	-0.57	24.92	26.66
34.15	+2.11	-0.72	25.57	27.31
35.14	+2.05	-0.34	23.95	25.68
36.13	+2.26	-0.57	24.95	26.68
37.01	+2.57	+0.29	21.19	22.93
37.56	+2.84	+1.46	16.13	17.87
38.45	+2.58	+0.87	18.67	20.40
38.89	+2.23	+0.57	20.00	21.74
39.44	+2.08	-0.02	22.55	24.29
40.21	+2.08	-0.16	23.17	24.91
40.87	+1.88	-0.29	23.75	25.48
41.86	+1.65	-0.61	25.09	26.83
42.41	+1.79	-0.78	25.83	27.57
42.85	+1.78	-0.80	25.94	27.68
43.73	+2.69	+1.06	17.88	19.61
44.50	+2.79	+1.55	15.73	17.46
44.95	+2.29	-0.02	22.57	24.31
45.50	+2.47	+0.21	21.57	23.30
46.16	+2.33	-0.20	23.31	25.05

46.71	+2.44	-0.31	23.79	25.53
47.37	+2.01	-0.46	24.47	26.21
48.14	+2.08	-0.66	25.32	27.06
48.80	+2.70	-0.08	22.81	24.55
49.57	+2.60	+1.36	16.56	18.30
50.45	+2.24	+0.35	20.94	22.67
51.22	+2.17	-0.06	22.71	24.45
51.89	+1.94	-0.40	24.21	25.94
52.44	+1.93	-0.53	24.79	26.52
53.21	+1.87	-0.54	24.83	26.57
53.65	+2.62	+0.68	19.52	21.25
54.31	+2.89	+1.53	15.83	17.57

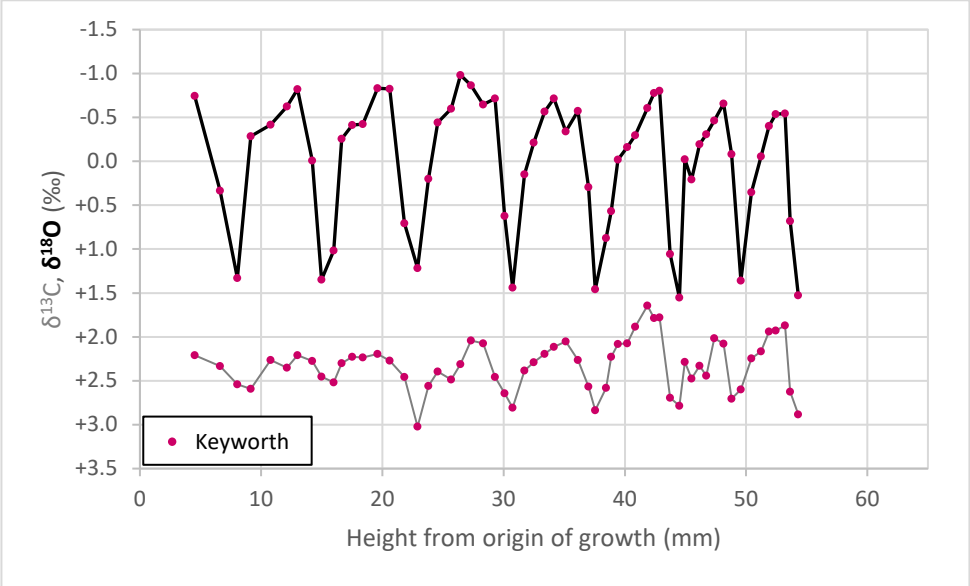

Summer $\delta^{18}O$ height: NA1

Year	Height (mm)
1	4.52
2	13.00
3	19.61
4	26.44
5	34.15
6	42.85
7	48.14
8	53.21

Shell data and calculated temperatures (Grossman and Ku): BC1

Height (mm)	$\delta^{13}C$ (‰)	$\delta^{18}O$ (‰)	Temp. ($\delta^{18}O_w$ = +0.7‰): BC1	Temp. ($\delta^{18}O_w$ = +1.1‰): BC1
1.70	+0.68	-0.52	24.73	26.46
3.24	+0.61	+0.27	21.28	23.02
4.34	-0.14	-0.04	22.66	24.39
5.30	-0.38	-0.21	23.36	25.10
6.24	-0.57	-0.43	24.33	26.07
7.20	-1.10	-0.33	23.91	25.64
7.88	-0.56	+0.01	22.43	24.17
8.52	-0.52	+0.16	21.77	23.51
9.36	-0.61	+0.05	22.25	23.99
10.08	-0.34	+0.24	21.41	23.15
10.91	-0.22	+0.58	19.94	21.67
11.74	-0.49	-0.87	26.23	27.96
12.32	-0.68	-1.11	27.27	29.00
13.11	-0.72	-0.92	26.47	28.20
13.92	-0.61	-0.75	25.74	27.48
14.69	-0.82	-0.62	25.15	26.89
15.34	-0.87	-0.55	24.84	26.58
16.00	-0.81	-0.65	25.27	27.01
16.68	-0.30	-0.31	23.80	25.53
17.39	+0.16	+0.18	21.70	23.43
18.38	+0.24	+0.90	18.55	20.29
19.10	+1.08	+0.48	20.39	22.13
19.66	+0.16	+0.17	21.74	23.48
20.22	-0.26	-0.04	22.65	24.38
20.84	-0.36	-0.37	24.09	25.83
21.54	-0.59	-0.63	25.18	26.92
22.23	-0.66	-0.76	25.76	27.49
22.76	-0.48	-0.62	25.17	26.90
23.35	-0.46	-0.66	25.32	27.05
23.98	-0.57	-0.44	24.38	26.11
24.62	-0.59	-0.51	24.67	26.41
25.20	-0.61	-0.21	23.37	25.11
25.73	-0.02	+0.70	19.41	21.15
26.41	+0.42	+1.42	16.31	18.04
26.98	+0.47	+1.08	17.79	19.53
27.71	+0.20	+0.85	18.79	20.52
28.18	+0.01	+0.71	19.37	21.10
28.87	+0.08	+0.78	19.10	20.84
29.46	+0.55	+0.89	18.60	20.34
30.02	+0.58	+0.70	19.41	21.15
30.42	+0.35	+0.57	20.01	21.75
31.03	+0.18	+0.61	19.81	21.55
31.65	-0.19	+0.35	20.94	22.67
32.21	-0.30	+0.15	21.81	23.54
32.75	-0.40	-0.04	22.65	24.39
33.33	-0.44	-0.27	23.63	25.37
33.85	-0.94	-0.63	25.20	26.94

34.38	-0.92	-0.38	24.10	25.83
35.05	-0.09	+0.32	21.09	22.83
35.58	+0.04	+0.60	19.85	21.58
36.12	+0.11	+0.96	18.30	20.04
36.66	+0.57	+1.35	16.63	18.36
37.29	+0.11	+0.45	20.52	22.26
37.85	+0.21	+0.81	18.96	20.70
38.35	+0.06	+0.49	20.34	22.08
39.00	-0.09	+0.49	20.36	22.10
39.52	-0.44	+0.62	19.78	21.51
40.25	-0.55	+0.69	19.46	21.19
40.92	-0.81	+0.60	19.88	21.62
41.62	-1.34	-0.51	24.67	26.41
42.21	-1.32	-0.53	24.79	26.52
42.80	-1.51	-0.40	24.19	25.92
43.37	+2.44	-0.63	25.22	26.96
43.98	+2.35	-0.37	24.09	25.82
44.67	+2.21	-0.08	22.80	24.54
45.36	+2.41	+0.05	22.26	24.00
45.96	+2.39	+0.18	21.66	23.40
46.56	+2.20	+0.43	20.61	22.35
47.18	+2.13	+0.48	20.38	22.11
47.61	+2.05	+0.34	20.98	22.71
48.14	+1.95	+0.46	20.47	22.21
48.79	-1.61	-0.55	24.86	26.59
49.51	-0.40	+0.40	20.72	22.45
50.12	-0.10	+0.87	18.67	20.41
50.77	+0.28	+0.82	18.93	20.66
51.94	+0.28	+1.07	17.81	19.54
53.08	-0.88	-0.98	26.74	28.48

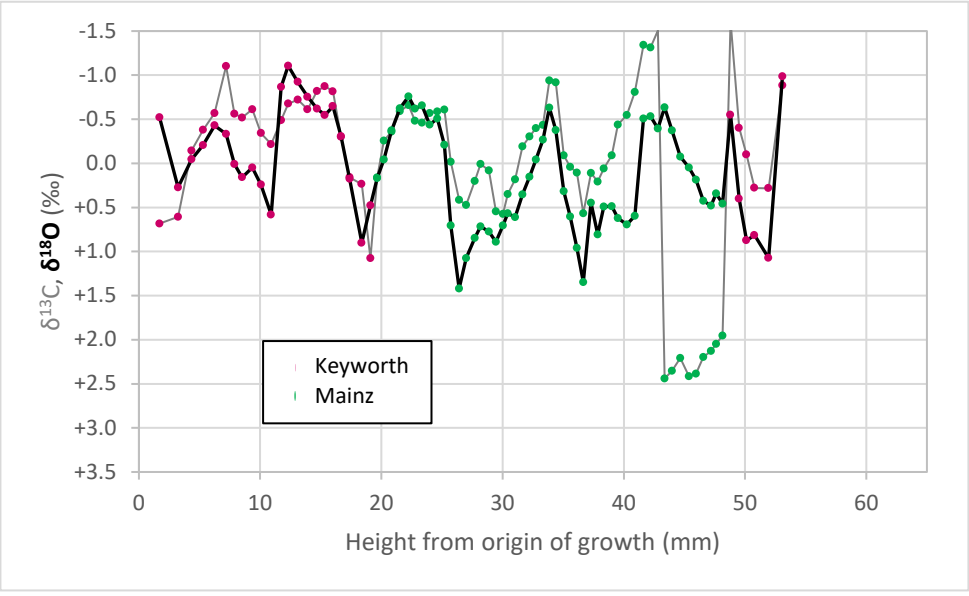

BC1

Size/cumulative size of hinge increments: BC1

Year	Inc. width (µm)	Cumulative inc. width (µm)	Cumulative inc. width (mm)
1	1639.94	1639.94	1.64
2	956.95	2596.89	2.60
3	1037.65	3634.54	3.63
4	1116.22	4750.77	4.75
5	1078.39	5829.16	5.83
6	696.64	6525.80	6.53
7	412.78	6938.59	6.94
8	491.04	7429.62	7.43
9	688.74	8118.36	8.12
10	442.08	8560.44	8.56
11	452.72	9013.17	9.01
12	275.63	9288.80	9.29
13	337.39	9626.19	9.63
14	296.67	9922.87	9.92
15	251.41	10174.28	10.17

Summer $\delta^{18}O$ height: BC1

Year	Height (mm)
1	1.7
2	6.24
3	12.32
4	22.23
5	33.85
6	43.37
7	48.79
8	53.08